# Craniomandibular anatomy of the akidnognathid therocephalian *Olivierosuchus parringtoni* from the Early Triassic of South Africa

**Alessandro Gigliotti[1,2*§], Luisa C. Pusch[1,2], Christian F. Kammerer[3,4], Julien Benoit[4] & Jörg Fröbisch[1,2,4]**

[1]*Museum für Naturkunde, Leibniz-Institut für Evolutions- und Biodiversitätsforschung, Berlin, Germany*
[2]*Institut für Biologie, Humboldt-Universität zu Berlin, Berlin, Germany*
[3]*North Carolina Museum of Natural Sciences, Raleigh, NC, U.S.A.*
[4]*Evolutionary Studies Institute (ESI), University of the Witwatersrand, Johannesburg, South Africa*

Received 22 August 2023. Accepted 8 December 2023

Therocephalians were an ecomorphologically varied group of therapsids with global distribution during the late Permian and earliest Triassic periods. Here, we redescribe the holotype of the therocephalian *Olivierosuchus parringtoni* (BP/1/3849) from the Early Triassic *Lystrosaurus declivis* Assemblage Zone in the main Karoo Basin of South Africa. The specimen includes a complete skull, mandible, and the anterior portion of the skeleton. Previously unknown endocranial features are described using high-resolution computed tomography (CT), including internal surfaces of the braincase and palatal bones, as well as structures deriving from soft tissues such as the brain and inner ear endocasts. Comparisons with closely related therapsids permit a detailed comparative analysis of the brain and inner ear morphology of *Olivierosuchus*. Both structures show a close resemblance to other early therapsid taxa.

**Key words**: Synapsida, Therocephalia, Permian, Triassic, Karoo Basin, CT data.



## INTRODUCTION

Therocephalia is one of the major subclades of Therapsida, the mammal-like synapsids that dominated terrestrial vertebrate assemblages from the middle Permian to the Middle Triassic. Therocephalia represents the sister-group of Cynodontia, and later representatives of this clade convergently evolved many of the 'mammal-like' features seen in cynodonts, including a complete secondary palate and complex crown-to-crown occlusion of the postcanine teeth (Huttenlocker 2009). The earliest therocephalians are known from the *Eodicynodon* Assemblage Zone (AZ) in the Karoo Basin of South Africa (Abdala *et al*. 2008; Kammerer 2023) and showed a general resemblance to Gorgonopsia. These early therocephalians were relatively large (skull lengths about 20–30 cm), 'sabre-toothed' animals, and were among the most abundant tetrapod predators of the middle Permian in South Africa (Smith *et al*. 2012). Although the main groups of large-bodied, macropredatory therocephalians (Lycosuchidae and Scylacosauridae) died out soon after the end of the middle Permian (Day & Rubidge 2021), the surviving group of therocephalians (Eutherocephalia) underwent a major radiation, and the group reached the peak of its diversity in the late Permian (Huttenlocker & Smith 2017; Day & Smith 2020). In addition to high species richness, late Permian therocephalians also showed high ecomorphological variation, including small-bodied, probably insectivorous morphotypes, some taxa with remarkable cranial bosses (Benoit *et al*. 2016b) and a possible venomous bite (Benoit *et al*. 2017c), as well as the re-evolution of macropredatory forms (Brocklehurst 2019).

Despite their great morphological variability, there are a few characteristics that are present across therocephalians (Huttenlocker 2009). One of these is the medial enlargement of the temporal fenestra, reducing the intertemporal skull roof to a narrow bar. This feature is shared with cynodonts and represents one of the characters supporting their sister-group relationship in the more inclusive clade Eutheriodontia. Other important therocephalian characters (present in most taxa) include the paired suborbital vacuities in the palate, the broad vomer, and the absence of a dorsal process in the unperforated stapes. Additionally, in the lower jaw the reflected lamina of the angular combines a free dorsal margin with a series of strong ridges radiating from the central region (Kemp 2005; Olroyd & Sidor 2022). Within Eutherocephalia, three major lineages are currently recognized: Akidnognathidae, Whaitsioidea, and Baurioidea (Huttenlocker & Smith 2017). The Akidnognathidae can be distinguished from other therocephalian families by their conservative incisor count (five upper and four lower incisors), facial

*Author for correspondence. E-mail: alessandro.gigliotti@mfn.berlin

***Palaeontologia africana* 56**: 142–170 — ISSN 2410-4418 [Palaeontol. afr.] Online only
Permanently archived on the 15th of December at the University of the Witwatersrand, Johannesburg, South Africa
The article is permanently archived at: https://hdl.handle.net/10539/37185

enlargement of the septomaxilla, and a transverse expansion of the anterior margin of the vomer (Hopson & Barghusen 1986; van den Heever 1994; Huttenlocker 2009). Akidnognathid taxa vary extensively in body size; although the majority of these taxa were small animals with skull lengths of about 10 cm, some members of this family (e.g. *Moschorhinus*) comprised some of the largest tetrapod predators in the latest Permian and earliest Triassic (Kammerer *et al*. 2023).

Therocephalians, like most other synapsids, suffered substantial losses in the Permo-Triassic mass extinction event (PTME) (Grunert *et al*. 2019; Viglietti *et al*. 2021). However, therocephalians remained abundant, with relatively high species richness, in the Early Triassic South African recovery fauna (Smith & Botha-Brink 2014; Angielczyk & Kammerer 2018). With this said, Early Triassic members of the group show signs of strong selection pressure, probably due to resource scarcity (Huttenlocker 2014), resulting in a Lilliput effect (body-size reduction). The majority of earliest Triassic (*Lystrosaurus declivis* AZ) therocephalians in South Africa are baurioids, such as *Regisaurus* and *Scaloposaurus* (Huttenlocker *et al*. 2022). This group would go on to radiate anew, becoming the only therocephalian clade to undergo diversification in the Triassic in the form of the highly specialized, predominantly herbivorous subclade Bauriamorpha. By contrast, akidnognathids do not appear to have survived beyond the Early Triassic (e.g. Huttenlocker 2009; Huttenlocker *et al*. 2011; Huttenlocker & Sidor, 2017). Although they represent an important component of *Lystrosaurus declivis* AZ faunas (Huttenlocker *et al*. 2011), this group can be considered a 'dead clade walking' as they did not diversify again following the PTME. Two *Lystrosaurus declivis* AZ akidnognathid species are known from extensive and well-preserved fossils: *Moschorhinus kitchingi* and *Olivierosuchus parringtoni*.

Unlike *Moschorhinus*, which is the largest known akidnognathid, *Olivierosuchus parringtoni* represents one of the smaller representatives of its clade, with the largest known specimen (NMQR 3605) exhibiting a total skull length of 117 mm. This species was first described by Brink (1965) based on a complete skull with occluded lower jaws and articulated anterior postcranium (BP/1/3849). Originally given the genus name *Olivieria*, this proved to be homonymous with an extant fly and was renamed *Olivierosuchus* by Kammerer & Sidor (2002), after the type locality Oliviershoek Pass and the Ancient Greek word for crocodile. Seven specimens of *O. parringtoni* are currently known in South African museum collections (Table 1). Four specimens were listed by Botha-Brink & Modesto (2011) in their description of NMQR 3605. An additional, nearly complete skeleton (BP/1/3973), misidentified as the baurioid *Regisaurus jacobi* by Fourie & Rubidge (2007), was referred to *O. parringtoni* by Botha-Brink *et al*. (2014). Huttenlocker & Botha-Brink (2014) presented osteohistological data for NQMR 3605 and another, otherwise undescribed *O. parringtoni* skeleton (SAM-PK-K10617). To these can be added a well-preserved, unnumbered skull in the collections of the Council for Geoscience (Fig. 1B,E). *Olivierosuchus parringtoni* is one of the few taxa that ranges throughout the *Lystrosaurus declivis* AZ, indicating that it was a persistent component of the Early Triassic recovery fauna in South Africa (Botha & Smith 2020).

**Table 1**. List of *Olivierosuchus parringtoni* specimens.

| Specimen number | Locality |
|---|---|
| BP/1/3849 | New Castle of the Admiralty Estates, Oliviershoek Pass, Bergville, KwaZulu-Natal |
| BP/1/3973 | Nooitgedacht 68, Bethulie, Free State |
| CGS unnumbered | Unknown |
| NMQR 62 | Zeekoeigat, Venterstad, Eastern Cape |
| NMQR 3605 | Barendskraal, Middelburg, Eastern Cape |
| SAM-PK-K117 | Skerpioenkraal, Middelburg, Eastern Cape |
| SAM-PK-K10617 | Wapadsberg Pass, Graaff-Reinet, Eastern Cape |

Brink (1965) initially placed *'Olivieria'* in the 'scaloposaurian' family Ictidosuchidae and considered it to be most closely related to the genera *Ictidosuchoides* and *Ictidosuchops*. Brink's (1963, 1965) classification of the 'higher' theriodonts differed strongly from the modern consensus, treating Scaloposauria as a therapsid suborder distinct from and equal in rank to Therocephalia (see also Watson 1931; Boonstra 1972). Hopson & Barghusen (1986) recognized 'Scaloposauria' as an unnatural group made up mostly of various juvenile therocephalians, classifying the core 'scaloposaurs' (e.g. *Scaloposaurus* itself) within the therocephalian superfamily Baurioidea. Brink (1986) did later consider *'Olivieria'* to be a therocephalian (within his 'Order Therocephalida'), and shifted its familial attribution from Ictidosuchidae to Nanictidopsidae, the latter constituting a motley assemblage of taxa currently classified as scylacosaurids (e.g. *Blattoidealestes*, *Crapartinella*; Kammerer 2023), akidnognathids (e.g. *Promoschorhynchus*; Huttenlocker *et al*. 2011), hofmeyriids (e.g. *Hofmeyria*, *Ictidostoma*; Huttenlocker & Smith 2017), and baurioids (e.g. *Choerosaurus*; Sigurdsen *et al*. 2012). Identification of *Olivierosuchus* as an akidnognathid was first suggested in the work of Colbert & Kitching (1981), who believed the holotype of *O. parringtoni* to represent a juvenile specimen of *Moschorhinus*. This proposal has not been supported by subsequent studies (e.g. Botha-Brink & Modesto 2011), but their recognition of similarities between these taxa was perceptive, and the two were recovered as close relatives in the first computer-assisted cladistic analysis focused on Therocephalia (Huttenlocker 2009), with both considered members of the clade Akidnognathidae.

Subsequent phylogenetic analyses have all supported an akidnognathid position for *Olivierosuchus* (e.g. Sigurdsen *et al*. 2012; Huttenlocker *et al*. 2011, 2015; Huttenlocker & Sidor 2016; Huttenlocker & Smith 2017; Liu & Abdala 2017, 2019, 2022, 2023; Kammerer & Masyutin 2018; Sidor *et al*. 2022), but the exact interrelationships within this clade, especially among small-bodied South African taxa, require additional study. *Olivierosuchus* has fairly consistently been recovered as the sister-taxon of *Promoschorhynchus* (e.g. Huttenlocker 2009), but the highly specialized *Euchambersia* has proven more labile, being recovered as a relatively basal akidnognathid in early analyses (e.g. Huttenlocker *et al*. 2011) but

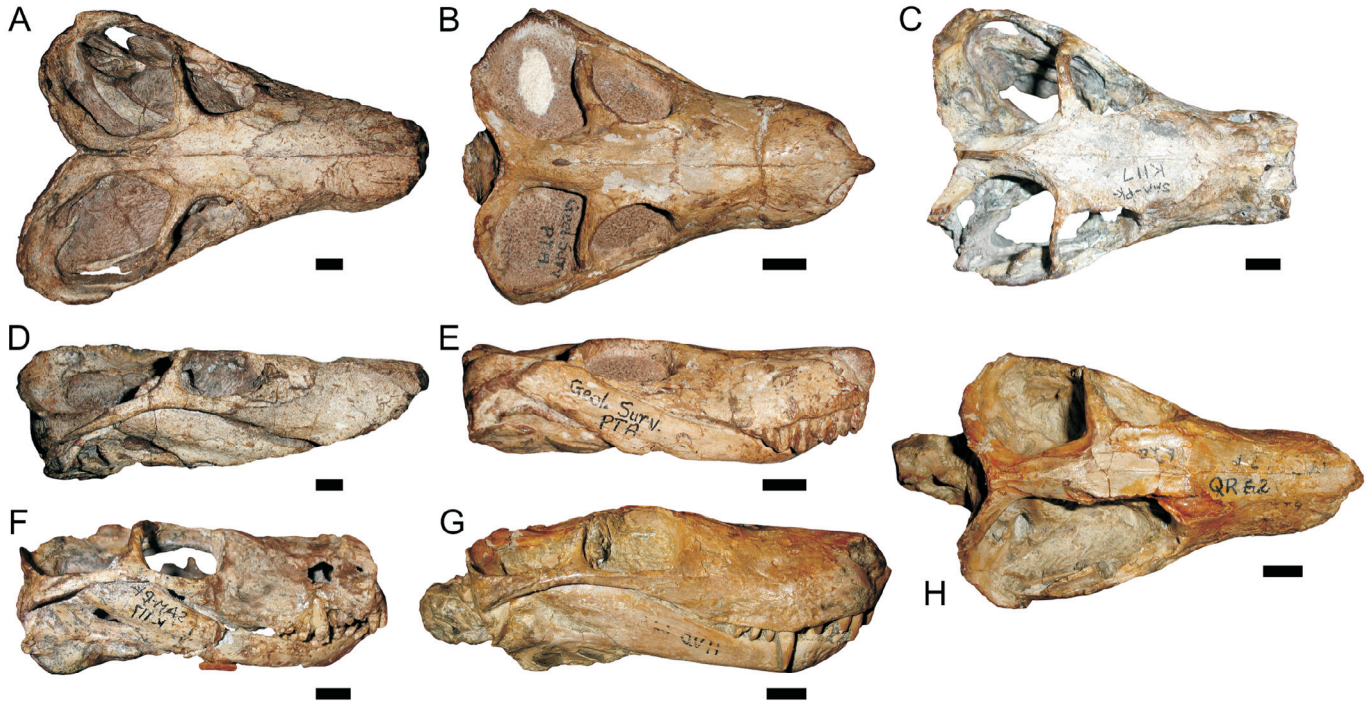


**Figure 1**. Referred crania of *Olivierosuchus parringtoni*. NMQR 3605 in **A**, dorsal and **D**, right lateral views. Unnumbered CGS specimen in **B**, dorsal and **E**, right lateral views. SAM-PK-K117 in **C**, dorsal and **F**, left lateral views (lateral view mirrored for comparative purposes). NMQR 62 in **G**, left lateral (mirrored) and **H**, dorsal views. Scale bars represent 1 cm.

more recently as a deeply-nested taxon related to *Moschorhinus* (e.g. Liu & Abdala 2022). The alpha taxonomy of this group also requires revision, with potential implications for phylogenetic topology depending on whether nominal genera such as *Cerdops*, *Cerdosuchoides*, *Cerdosuchus*, *Notaelurodon*, and *Zorillodontops* are actually distinct from *Akidnognathus* and *Promoschorhynchus*.

Previous studies on *O. parringtoni* mostly involved description of its external anatomy (e.g. Brink 1965; Botha-Brink & Modesto 2011) or osteohistology (Huttenlocker & Botha-Brink 2014). A few papers have addressed neuroanatomical aspects of this species: Findlay (1968) described the externally visible facial foramination of BP/1/3849, associating the maxillary foramina with branches of the infraorbital nerve, and Benoit *et al*. (2016a, 2018) investigated the evolution of the maxillary canals housing the infraorbital nerve across Therapsida, including reconstructions of these canals in *Olivierosuchus* based on computed tomographic (CT) data. However, much of the internal anatomy of the *O. parringtoni* cranium remains undescribed. Here, we provide the first comprehensive examination of endocranial characters in this taxon, describing the brain endocast, bony labyrinth, and internal bone morphology on the basis of a CT-reconstruction of the holotype, BP/1/3849.

## MATERIAL AND METHODS

### Specimen

The specimen described herein (BP/1/3849) is part of the collection of the Evolutionary Studies Institute (ESI) at the University of the Witwatersrand in Johannesburg. BP/1/3849 was recovered from the farm New Castle, formerly an annex of Admiralty Estates, uThukela District Municipality (former Bergville District), KwaZulu-Natal Province, in the northeastern part of the Karoo Basin (Botha-Brink & Modesto 2011). Botha-Brink & Modesto (2011) stated that because BP/1/3849 was recovered from the same locality and stratigraphic horizon as the holotype of *Tetracynodon darti* (BP/1/2710) (Brink 1965), it must have originated in the Harrismith Member of the Normandien Formation (equivalent to the Palingkloof Member of the Balfour Formation; Rubidge 1995; Botha & Smith 2020).

BP/1/3849 consists of an almost completely preserved skull with occluded lower jaw (Figs 2–4) and the anterior half of the skeleton in articulation, including vertebrae, ribs, pectoral girdle, partial left humerus, and the complete right forelimb with terminal phalanges. The following description is based on the portion of the skeleton that was CT-scanned, consisting of the cranium, lower jaw, and the two cervical vertebrae articulated to the cranium (the left atlantal neural arch and possible broken anterolateral edge of the atlas pleurocentrum). The skull is 110 mm long, 66 mm wide, and approximately 35 mm high. The cranium, lower jaw, and dentition of BP/1/3849 are generally well preserved, though the snout, orbital region, parts of the skull roof, and mandible are marked by cracks. The left side of the snout also appears slightly compressed (Fig. 4).

### Computed tomography data

BP/1/3849 was CT-scanned at the scanning facility of the University of the Witwatersrand Palaeosciences Centre using a Nikon Metrology XTH 225/320 LC dual source CT system with 2500 projections and a voxel size of 0.0655 mm, a voltage of 135 kV, and a current of 200 $\mu$A. In addition, a copper filter was applied with a thickness of 1.2 mm.

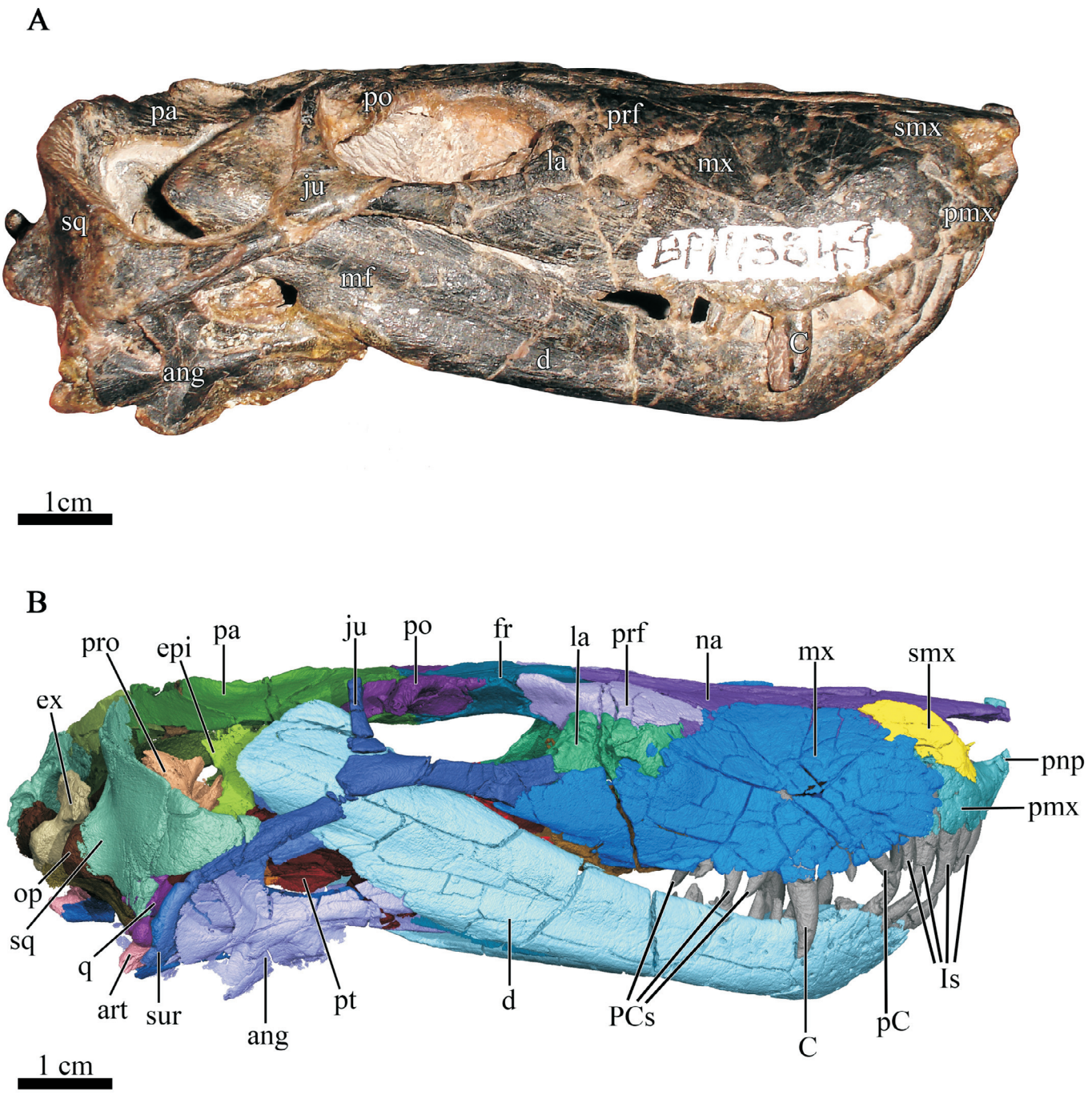


**Figure 2**. Skull of BP/1/3849, the holotype of *Olivierosuchus parringtoni*, in right lateral view. **A**, Photograph and **B**, 3D reconstruction of the skull. *Abbreviations*: ang, angular; art, articular; C, upper canine; d, dentary; epi, epitperygoid; ex, exoccipital; fr, frontal; Is, upper incisors; ju, jugal; la, lacrimal; mx, maxilla; na, nasal; op, opisthotic; pa, parietal; pC, upper precanine; PCs, upper postcanines; pmx, premaxilla; pnp, prenasal process of the premaxilla; po, postorbital; prf, prefrontal; pro, prootic; pt, pterygoid; q, quadrate; smx, septomaxilla; sq, squamosal; sur, surangular.

The visualization of the slices, virtual 3D rendering, segmentation, and measurements of selected structures were performed using VGStudio Max 3.4 (Volume Graphics GmbH, Heidelberg, Germany) in the 3D Visualization Laboratory at the Museum für Naturkunde Berlin. The digital segmentation and reconstruction of the brain and inner ear endocasts were performed on the sediment infilling the brain cavity and bony labyrinth of the skull, respectively. The measurements of the bony labyrinth follow the protocol of Benoit *et al*. (2017b).

**Brain endocast volume, body mass, and EQ**

Endocranial volume measurements of BP/1/3849 were also taken using VGStudio Max 3.4. The synapsid encephalization quotient (EQS) of *Olivierosuchus* was calculated using the method of Benoit *et al*. (2023). We also estimated the EQS for the recently redescribed Early Triassic cynodont *Nythosaurus lavatus* based on the brain endocast volume calculated by Pusch *et al*. (2023). For these, the average body mass of both taxa was calculated by using the method from Benoit *et al*. (2017d). The newly calculated data were incorporated into the dataset of Benoit *et al*. (2023) (Table 2). An EQS value of 1 means that a given species has exactly an average brain size for a non-Cenozoic synapsid of its given body mass.

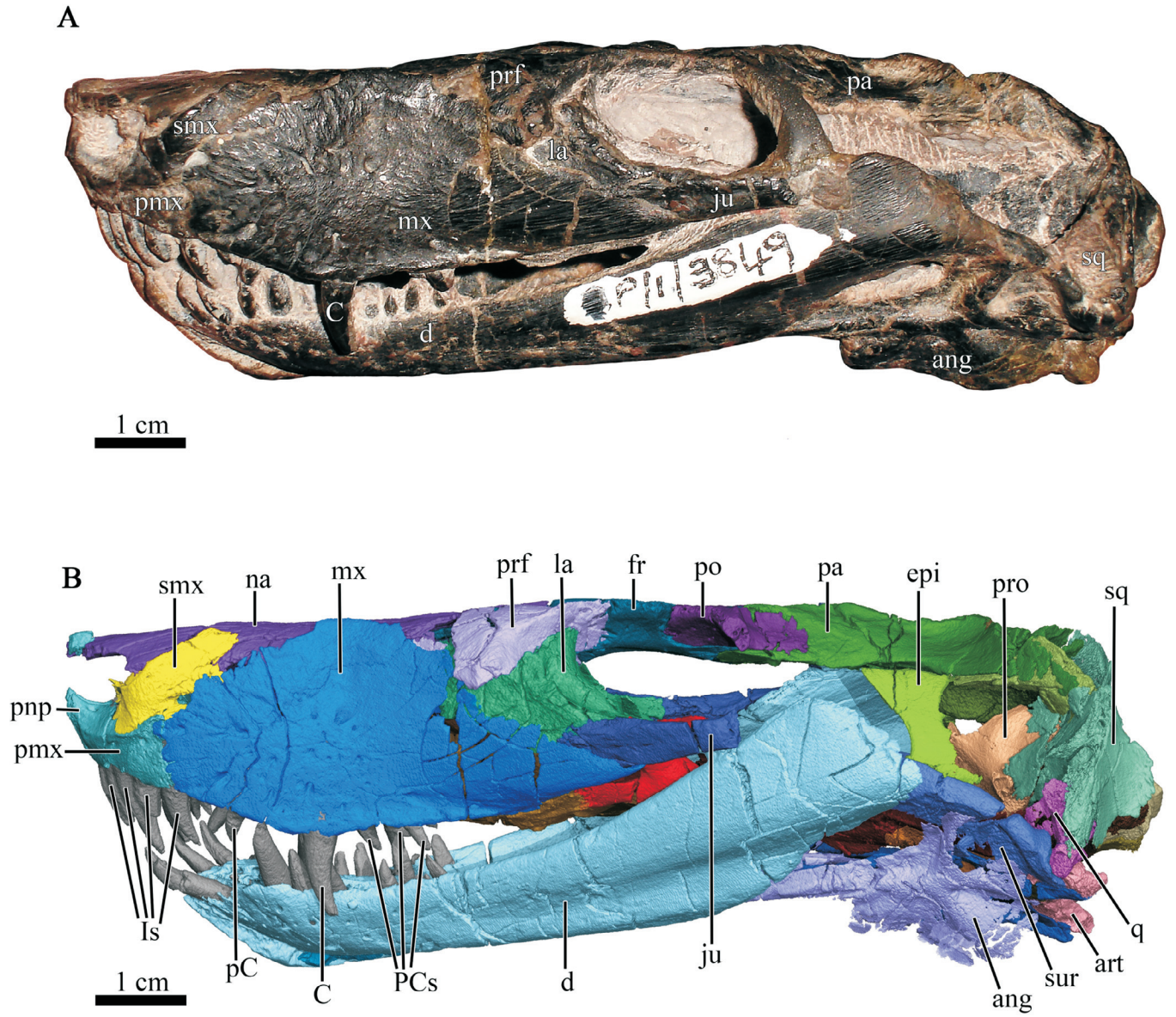


**Figure 3**. Skull of BP/1/3849 in left lateral view. **A**, photograph and **B**, 3D reconstruction of the skull. *Abbreviations*: ang, angular; art, articular; C, upper canine; d, dentary; epi, epitperygoid; fr, frontal; Is, upper incisors; ju, jugal; la, lacrimal; mx, maxilla; na, nasal; pa, parietal; pC, upper precanine; PCs, upper postcanines; pmx, premaxilla; pnp, prenasal process of the premaxilla; po, postorbital; prf, prefrontal; pro, prootic; q, quadrate; smx, septomaxilla; sq, squamosal; sur, surangular.

## RESULTS

### General preservation

The skull of BP/1/3849 is missing parts of the anterior-most tip of the snout, comprising portions of the prenasal (intranarial) process of the premaxilla and the anterior-most portion of the left nasal bone, as well as most of the left postorbital bar and posterior zygomatic arch (Figs 2–5). The external surface of the right maxilla is more strongly cracked than that of the left maxilla, with a number of fissures concentrated around the level of the canine. In addition, the anterior margin is slightly damaged in both maxillae. Posteriorly, the dorsal lamina of the maxilla is damaged on both sides, exposing internal portions of the lacrimals and nasals that would have been covered by the maxillae when intact (Figs 2, 3, 5, 6). The nasals are strongly cracked near their midline suture. By contrast, the frontal bones are in much better condition, albeit slightly separated at their midline suture (Fig. 7). As the left postorbital bar is reconstructed in plaster in BP/1/3849, it could not be visualized in the CT data and thus is not reconstructed for the specimen (Figs 3, 4). The palate is well preserved, with only the anterior portion of the vomer being damaged (Fig. 8). The braincase is also generally in good condition, but some bones are slightly deformed and have been shifted inside the braincase. For instance, the sphenethmoid is preserved, but not in its original position (Fig. 9). The dorsal occipital plate is compressed, with the result that the dorsal portion of the supraoccipital has been strongly shifted into the brain cavity (Fig. 10). The dorsal portion of the ascending process of the left epipterygoid has also shifted into the brain cavity. The right prootic and opisthotic bones are slightly damaged, and the better preserved left prootic has slightly been shifted upwards due to deformation (Figs 11, 12C). Two cervical bones, the left atlantal neural arch and possible broken anterolateral edge of the atlas pleurocentrum, are preserved in articulation with the

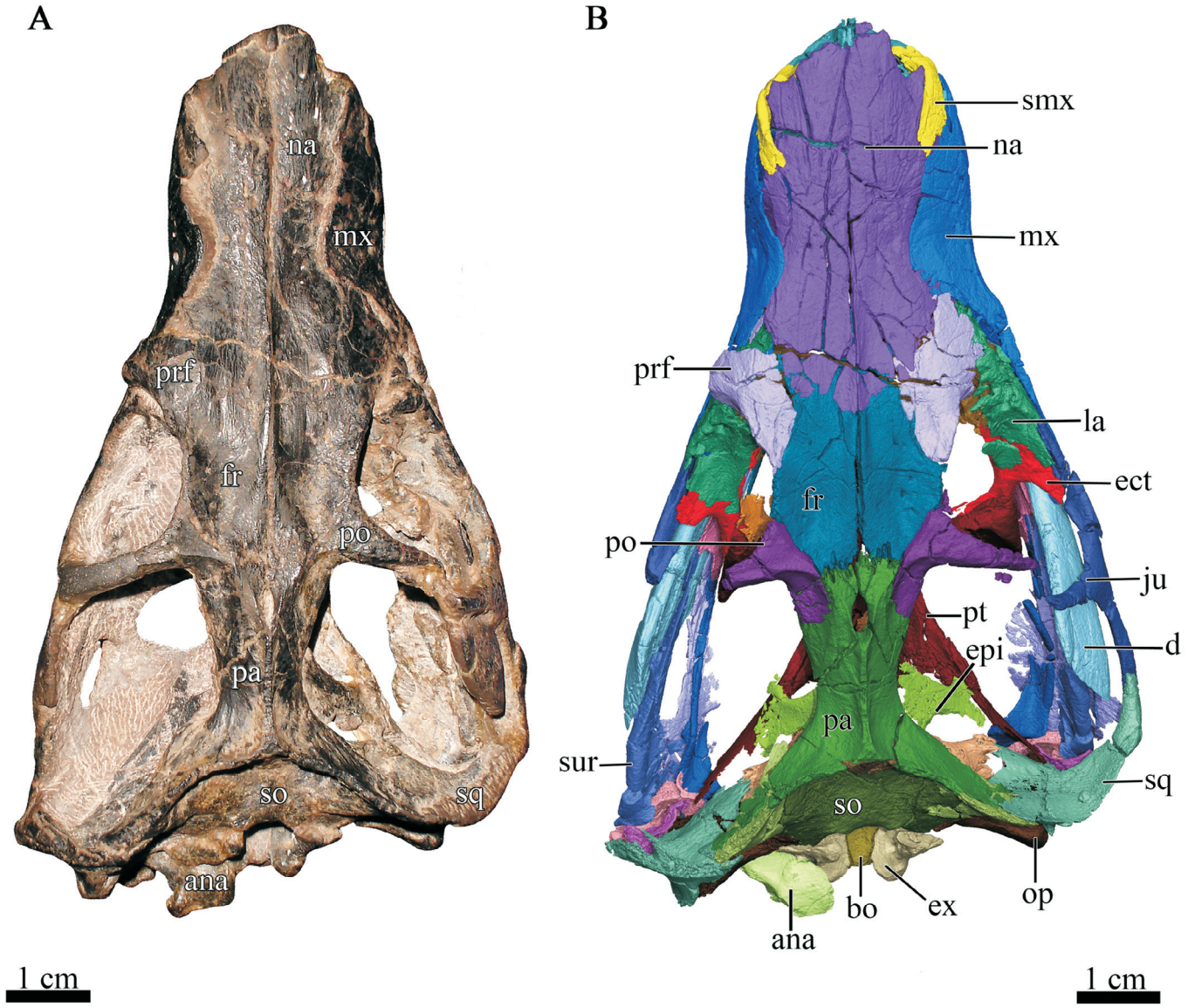


**Figure 4**. Skull of BP/1/3849 in dorsal view. **A**, photograph and **B**, 3D reconstruction of the skull. *Abbreviations*: ana, atlantal neural arch; bo, basioccipital; d, dentary; ect, ectopterygoid; epi, epipterygoid; ex, exoccipital; fr, frontal; ju, jugal; la, lacrimal; mx, maxilla; na, nasal; op, opisthotic; pa, parietal; po, postorbital; prf, prefrontal; pt, pterygoid; smx, septomaxilla; so, supraoccipital; sq, squamosal; sur, surangular.

skull (Fig. 12B). The stapedes and hyoids are missing entirely in BP/1/3849. The lower jaw is relatively well preserved (Figs 2, 3, 13), although the posterior portion of the right splenial and the anteriormost portions of the right angular, prearticular, and surangular are missing. In addition, the posterior portion of the left surangular contacting the angular is damaged on the left side.

## Snout

*Premaxilla*

The premaxilla forms the anteromedial border of the external naris (Figs 2, 3). Its characteristic prenasal (intranarial) process is badly damaged in BP/1/3849, but a small piece of its dorsal process is preserved, extending slightly between the nasals (Figs 3, 5). What is preserved of the prenasal process shows that *Olivierosuchus* has a pointed snout tip, with the dorsal portion of the premaxilla extending more anteriorly than the ventral portion (also seen in the CGS specimen, which is the only *O. parringtoni* skull preserving an intact prenasal process; Fig. 1B,E). Two circular foramina are situated near the base of the prenasal process in each premaxilla: the first (the larger of the two) on the anterior face of the premaxilla above the first incisor and the second on the anteroventral floor of the external naris (Fig. 5). These might have served as the passage for the nasopalatine nerve and vessels. The premaxilla is overlapped by the septomaxilla dorsolaterally and by the maxilla posterolaterally up to the level of the fourth incisor (I4) (Fig. 6B). A shallow, elongated depression is present on the external surface of the premaxilla ventral to its contact with the septomaxilla; this groove houses two additional foramina comparable in size to the one in the narial floor (Figs 3, 5). The palatal surface of the premaxilla (Fig. 8B) is mostly flat, although immediately posterior to the functional incisors is a series of pits for the replacement incisors (see section on Dentition and Tooth Replacement below). Posterior to this series are two sets of paired foramina; on the ventral surface of each premaxilla is a circular foramen

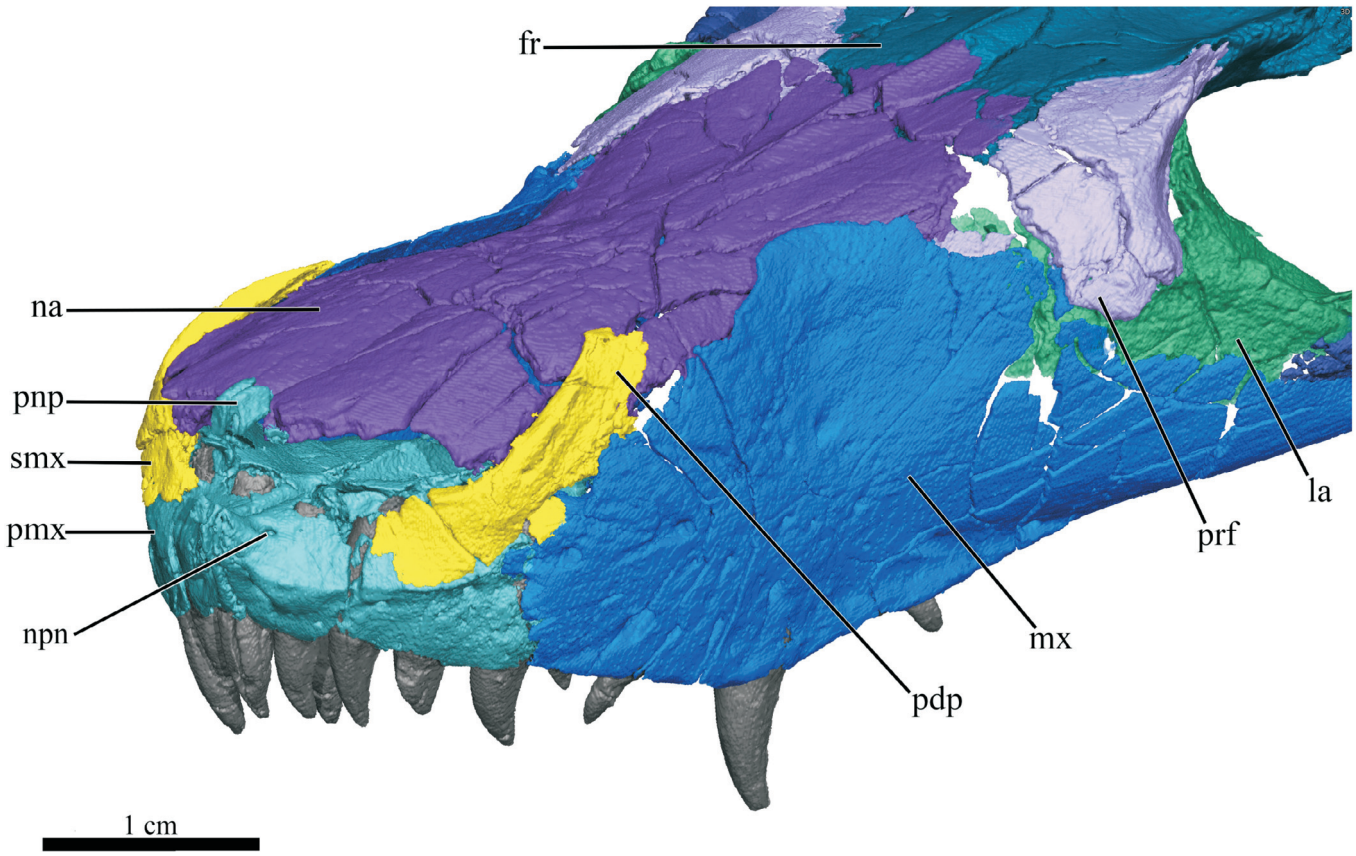


**Figure 5**. Three-dimensional reconstruction of the anterior portion of the snout of BP/1/3849 in left anterodorsolateral view. *Abbreviations*: fr, frontal; la, lacrimal; mx, maxilla; na, nasal; npn, nasopalatine nerve opening; pdp, posterodorsal process of the septomaxilla; pmx, premaxilla; pnp, prenasal process of the premaxilla; prf, prefrontal; smx, septomaxilla.

near the mid-premaxillary suture and a smaller, oval foramen posterolateral to it. An additional pair of much smaller foramina is present posterior to the more medial set, near the contact with the vomer. Dorsally, the palatal portion of the premaxilla is broadly depressed, with this depression narrowing anteromedially and being bounded medially by a sharp ridge at the mid-premaxillary suture (Fig. 8A). A single, median foramen is present anteriorly (immediately posterior to the tooth row); this would have ramified internally and connected to the foramina exposed ventrally. Posteromedially, the premaxilla-vomer contact is damaged, making it difficult to determine its exact morphology in BP/1/3849 (Fig. 8). Based on the preserved morphology of other *Olivierosuchus* specimens (Botha-Brink & Modesto 2011), however, it can be inferred to have been a broad ventral overlap of the vomerine process of the premaxilla by the anterior portion of the vomer, as is the case in other akidnognathids (Huttenlocker 2009).

*Septomaxilla*

The septomaxilla is relatively large (in comparison with therocephalians generally, but typical for akidnognathids), with extensive facial exposure, and forms the ventral and posterior border of the external naris (Figs 2–5). Its posterior two-thirds forms a long, posterodorsally oriented facial process that extends between nasal and maxilla. Its posterior terminus overlaps the ventral margin of the nasal. Its anteroventral portion is transversely expanded and forms a footplate situated on a flattened platform on the premaxillary surface within the external naris. A small, thin, anterodorsally protruding intranarial process is visible on the anteriormost margin of the septomaxilla. The septomaxillary foramen is relatively small (compared to e.g. *Moschorhinus*) and forms an oval opening, angled anteroventrally-to-posterodorsally, between the septomaxilla and the maxilla. This foramen forms the anterior terminus of the septomaxillary canal.

*Maxilla*

The maxilla is a large bone that forms a major part of the lateral surface of the snout and the sidewall of the nasal cavity. Its ventral margin is weakly convex, with an apex at the upper canine. Anteriorly, it contacts the septomaxilla and overlies the posterolateral margin of the premaxilla (Figs 2–5). The maxilla bears a long, triangular posterolateral process, which tapers up to the level of the middle of the orbit. The tip of this process underlies the anteroventral margin of the jugal (Fig. 8B). The morphology of this process is comparable to that of most other akidnognathids (e.g. Mendrez 1974; Huttenlocker *et al*. 2011), but differs from that of *Moschorhinus*, in which the posterolateral process has a tall, rounded contribution to the suborbital zygoma that overlaps the jugal laterally (Durand 1991: fig. 14). Dorsally, the maxillae of BP/1/3849 have a long, sinuous border with the nasals and broadly overlap them at the level of their greatest height, so that the nasals appear constricted in the middle (Fig. 4). By contrast, in the akidnognathid *Euchambersia*, the

maxilla-nasal suture is very short, and the nasal appears widest at the dorsal apex of the maxilla (Liu & Abdala 2022). The posterior margin of the maxilla is weakly concave where it contacts the prefrontal and lacrimal (Fig. 3).

The external surface of the left maxilla of BP/1/3849 is perforated by a number of small, circular foramina, concentrated mostly at the level of the upper canine (Figs 3, 5), marking the openings of rami from the maxillary canal, which has already been described by Benoit *et al*. (2016a, 2018). These foramina are also present in the right maxilla, but are only poorly visible due to damage of the external bone surface (Fig. 2). In addition to the foramina, the maxillary surface bears a variety of ridges and grooves, roughly radiating outwards from the canine region. The canine root is otherwise indistinct; the maxillary surface does not bulge outwards around it.

The internal surface of the facial portion of the maxilla is generally smooth and flat, but becomes thicker just anterior to its contact with the anterolateral process of the palatine, where it curves internally due to the large canine boss (Figs 6, 8). Anterior to the canine boss, there is a relatively small fossa located posterior to the septomaxilla and lateral to the vomerine process of the premaxilla, the anterior maxillary fossa (Fig. 6A,B). This fossa has also been described in the basal therocephalians *Alopecognathus* (van den Heever 1994; called *Glanosuchus* therein, but see Kammerer 2023) and *Lycosuchus* (Pusch *et al*. 2020) and the akidnognathid *Shiguaignathus* (Liu & Abdala 2017), but seems to be absent in the baurioid *Tetracynodon* (Sigurdsen *et al*. 2012). Immediately posterior to the canine boss, there is a second depression, called the posterior maxillary fossa by van den Heever (1994) or anterior maxillary sinus by Sigurdsen (2006). However, as previously suggested for the basal therocephalian *Lycosuchus* (Pusch *et al*. 2020), both the anterior and the posterior maxillary fossae might just be artefacts of the large medial development of the canine boss. Similar to basal therocephalians (Pusch *et al*. 2020), the large space posterior to the canine boss in BP/1/3849 is occupied by an extensive maxillary sinus (Fig. 6A), which has been reconstructed and figured for BP/1/3849 by Benoit *et al*. (2016a, 2018). Examination of this character in *Lycosuchus* (Pusch *et al*. 2020) and now *Olivierosuchus* accords with van den Heever's (1994) hypothesis that the posterior maxillary sinus in therocephalians is homologous with the maxillary sinus in cynodonts (e.g. Fourie 1974; Crompton *et al*. 2017; Pusch *et al*. 2019, 2021). Along its ventral margin, posterior to the canine boss, the maxilla contacts the palatine. The latter has a distinct anterolateral process, which extends dorsally just posterior to the canine boss to overlap the medial surface of the maxilla. Further posteriorly, a second process of the palatine, the medial process, rises even higher along the posteromedial surface of the maxilla to contact the lacrimo-palatine ridge of the lacrimal (Figs 6B,C, 8A). Dorsally, the internal surface of the maxilla is overlapped by the ventral margin of the nasal and posteriorly by the anterior margin of the lacrimal and the anterior process of the jugal.

*Nasal*

The elongated nasal bones form the roof of the snout and the nasal cavity. They extend anteriorly over the external naris, though the anteriormost portion of the left nasal bone is missing (Fig. 4). In dorsal view, the nasals are somewhat constricted at mid-length to give room for the curved, overlapping maxillae laterally, but flare out again to contact the frontals and the prefrontals at the level of the anterior margin of the orbit. The nasal-frontal suture appears roughly U-shaped, with the posterior margin of the nasals overlapping the anterior portion of the frontals. Though the posterior margin of the nasals is slightly damaged in BP/1/3849, this U-shaped suture is also clearly visible in the specimen of *Olivierosuchus* (NMQR 3605; Fig. 1A) described by Both-Brink & Modesto (2011). However, this suture is nearly straight in other specimens of *Olivierosuchus* (Fig. 1B,H), similar to that seen in *Euchambersia* (Liu & Abdala 2022) and *Moschorhinus* (Durand 1991). This morphology differs from that of the *Promoschorhynchus* specimen SAM-PK-K10014, in which the nasal-frontal suture is broadly W-shaped (Huttenlocker *et al*. 2011), with the anterior frontal margin convex (unlike the concave anterior margin in BP/1/3849). Mendrez (1974) described the presence of a low, mid-sagittal ridge on the dorsal surface of the frontals (continuing anteriorly onto the posterior portion of the nasals) in the akidnognathids *Promoschorhynchus* and *Moschorhinus*. A similar ridge also appears to be present in *Olivierosuchus* (Fig. 4B).

A series of faint, anteroposteriorly directed ridges extend along the ventral surface of the nasals and continue onto the frontals in BP/1/3849 (Fig. 7). These ridges are most strongly developed on the ventral surface of the frontals, and consist of a pair of lateral ridges running parallel to the midline suture of the nasal and frontal bones. A midline ridge would have existed along this suture when intact; although the ridge is not clearly visible due to displacement of the elements, the medial edges of these bones are slightly extended ventrally. Similar ridges have been described for a number of therapsids in recent years and have been interpreted as attachment sites for possible cartilaginous nasoturbinals, invoked for olfactory purposes (e.g. Kemp 1979; Hillenius 1991, 1994; Ruben 1996; Hillenius & Ruben 2004; Sigurdsen 2006; Ruben *et al*. 2012; Crompton *et al*. 2015, 2017; Bendel *et al*. 2018; Pusch *et al*. 2019, 2020, 2021; Huttenlocker & Sidor 2020).

*Lacrimal*

The lacrimal contributes to the anteroventral border of the orbit. As in all therocephalians except lycideopids (Sigurdsen *et al*. 2012), the dorsal lamina of the maxilla and the overlying prefrontal exclude the lacrimal from contacting the nasal externally. The slight external contact of the lacrimal with the nasal visible on the right side of the skull (Fig. 2) is due to damage of the maxilla and the prefrontal, which would have overlain the lacrimal and the nasal in that area when intact. Posteroventrally, the lacrimal is overlain by the anterior process of the jugal, which constitutes most of the ventral and posteroventral

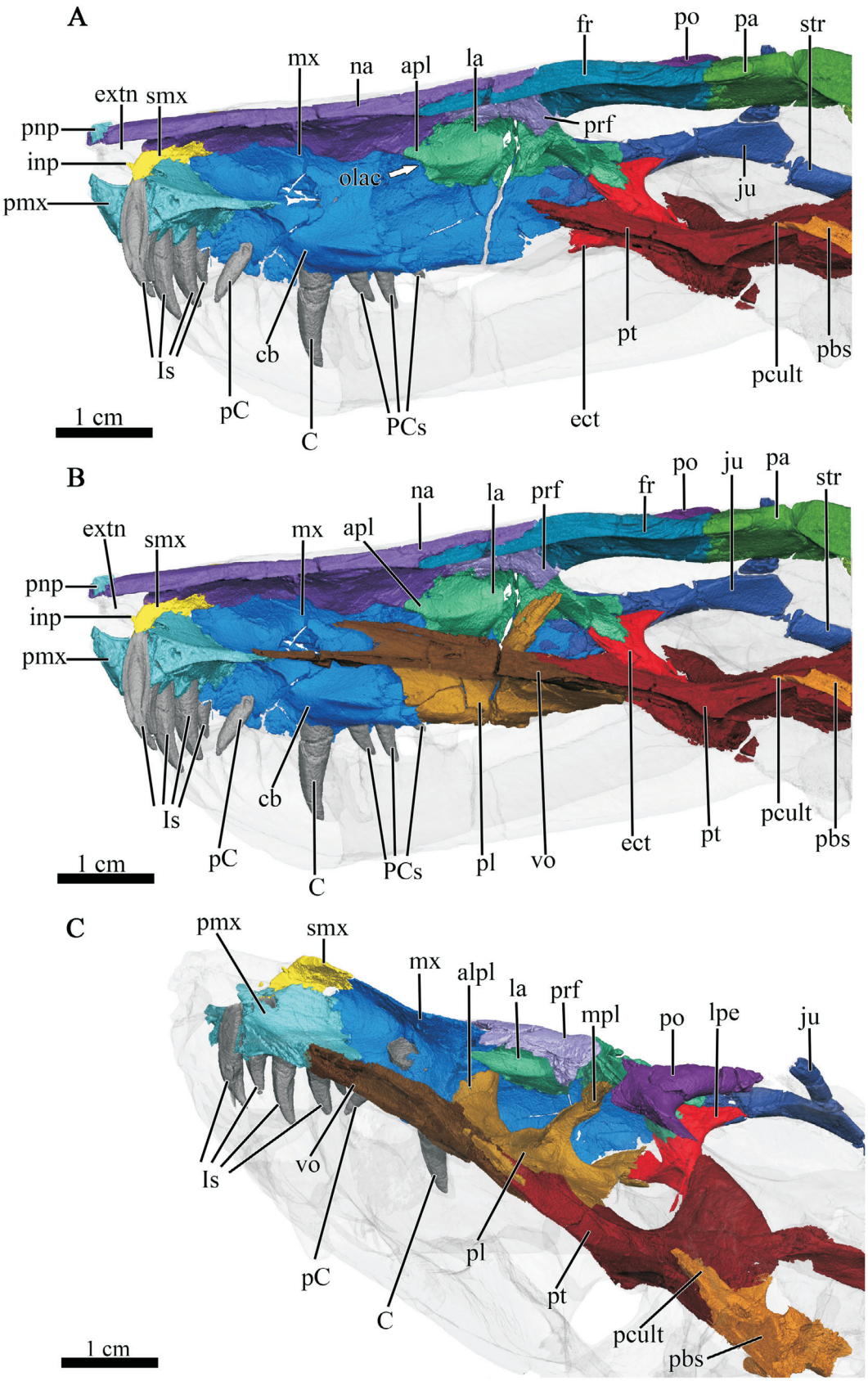


**Figure 6**. Mid-sagittal section through the snout of BP/1/3849 to show the internal morphology of the reconstructed nasal region. **A**, Internal view of the nasal region with the vomer and palatine digitally removed to expose the internal structure. **B**, Internal view of the nasal region with these bones not digitally removed. **C**, Internal morphology of the nasal region in right posterodorsolateral view with the skull roof digitally removed to expose the internal structure. *Abbreviations*: alpl, anterolateral process of the palatine; apl, anterior process of the lacrimal; C, upper canine; cb, canine boss; ect, ectopterygoid; extn, external naris; fr, frontal; inp, intranarial process of the septomaxilla; Is, upper incisors; ju, jugal; la, lacrimal; lpe, lateral process of the ectopterygoid; mpl, medial process of the palatine; mx, maxilla; na, nasal; olac, opening of the lacrimal canal; pa, parietal; pbs, parabasisphenoid; pC, upper precanine; PCs, upper postcanines; pcult, cultriform process of the parasphenoid; pl, palatine; pmx, premaxilla; pnp, prenasal process of the premaxilla; po, postorbital; prf, prefrontal; pt, pterygoid; smx, septomaxilla; str, subtemporal ramus of the jugal; vo, vomer.

part of the orbit (Figs 2–4). Internally, the lacrimal has a short anterior process contacting the posteroventral margin of the nasal (Fig. 6). A similar short anterior process of the lacrimal has been described for the lycideopid *Tetracynodon* (Sigurdsen *et al*. 2012). This contrasts with what was described in the supposed akidnognathid specimen PMO 206.702 by Sigurdsen (2006) and the basal therocephalians *Alopecognathus* (van den Heever 1994; Hillenius 1994; called *Glanosuchus* therein) and *Lycosuchus* (Pusch *et al*. 2020), in which the lacrimal has a long anterior process. However, unlike in PMO 206.702, *Glanosuchus*, and *Lycosuchus*, in which an internal contact of the lacrimal with the nasal only occurs along the anterior process, the lacrimal of BP/1/3849 has a broader contact with the nasal internally, occurring along its entire anterodorsal margin. This more closely resembles the morphology described for cynodonts, such as *Thrinaxodon* (Fourie 1974), *Galesaurus* (Pusch *et al*. 2019), and *Bolotridon* (Pusch *et al*. 2021), in which the lacrimal also has a broad contact with the nasal internally along its anterodorsal margin. Two foramina perforate the lacrimal posteriorly in the anterior margin of the orbit, through which the nasolacrimal duct originated. This structure proceeds through a ridge on the medial surface of the lacrimal and opens at the base of the short anterior process at the level of the third upper postcanine, above the expansive maxillary sinus (Fig. 6A). No obvious maxilloturbinal ridge can be seen beyond this opening, unlike what has been described for eucynodonts and potentially also some basal epicynodonts (e.g. Crompton 2013; Crompton *et al*. 2015, 2017; Pusch *et al*. 2019, 2021). On its medial surface, the lacrimal bears two ridges. The first of these ridges is the lacrimo-palatine ridge, which is nearly vertically oriented and contacts the thin, dorsally extending medial process of the palatine. The second ridge is the lacrimo-ectopterygoidal ridge, which proceeds internally from the posterodorsal margin of the lacrimal obliquely to its posteroventral margin to meet the ectopterygoid on the floor of the orbit.

*Jugal*

The jugal of BP/1/3849 is a relatively narrow, elongated bone that forms a major part of the posterolateral border of the orbit and the ventral portion of the zygomatic arch (Figs 2, 3, 4, 8). A comparable, relatively narrow morphology of the jugal has also been described for *Promoschorhynchus* (Mendrez 1974). By contrast, in *Moschorhinus* and *Euchambersia*, the jugal is a much more robust element, with a distinct, triangular ventral (suborbital) process (Durand 1991; Liu & Abdala 2022) that is absent in other akidnognathids.

Only the right jugal of BP/1/3849 is completely preserved, while for the left jugal only its anterior portion is present. The anterior extensions of both jugal bones overlap the posterior margins of the lacrimals and underlie the posteroventral processes of the maxillae. They bear a dorsal process midway along their length that would have contacted the descending rami of the postorbitals and contributed to the postorbital bars. On the right side of the skull, where these bones are preserved, this contact has been lost due to slight dislocation of the involved elements (Fig. 4). The posterior process of the jugal, also known as the subtemporal ramus, makes up the ventral border of the large temporal fenestra. The posterior process of the jugal extends posteriorly to meet the anteroventral process of the squamosal, which overlaps it dorsally, as can be seen on the right side of the skull (Figs 2, 4).

*Prefrontal*

The prefrontal forms the anterodorsal and part of the medial margin of the orbit (Figs 2–5). It contacts the maxilla anteriorly and the lacrimal ventrally. On the skull roof its dorsal margin curves inward to contact the nasal and to overlap the anterolateral portion of the frontal. The prefrontal overlies much of the dorsal margin of the lacrimal in external view, which is visible due to damage of the prefrontal especially on the right side of the skull, exposing a piece of the internal dorsal portion of the lacrimal (Fig. 2). In internal view, the prefrontal appears very small (Fig. 6), unlike in cynodonts such as *Thrinaxodon* (Fourie 1974), *Galesaurus* (Pusch *et al*. 2019), and *Bolotridon* (Pusch *et al*. 2021), in which the prefrontal has a descending flange internally, which overlies the lacrimal along its posteromedial margin. This structure is not visible in BP/1/3849; here the prefrontal only contacts the lacrimal along its dorsal margin.

**Skull roof**

*Frontal*

The frontals contribute to the roof of the skull at the level of the orbit (Fig. 4). The postorbital and the prefrontal almost exclude the frontal from the orbit, but the bone retains a short contribution to the margin of the dorsomedial border of the latter. Anteriorly, the frontals underlie the posterior margin of the nasals (Fig. 5) and posteriorly, they contact the parietals in an interdigitating suture (Figs 4, 7). Posterolaterally, the frontal meets the postorbital and anterolaterally, it is overlapped by the curved dorsal margin of the prefrontal. The general morphology of the frontals differs from that of *Moschorhinus* and *Euchambersia*, in which the frontals appear anteroposteriorly shorter and lateromedially wider (Durand 1991; Liu & Abdala 2022). Also, unlike in *Olivierosuchus* (Fig. 3; Botha-Brink & Modesto 2011) and its possible sister-taxon *Promoschorhynchus* (Huttenlocker *et al*. 2011), in which the frontal makes a moderate contribution to the dorsal orbital wall, the frontal of *Euchambersia* shows only a narrow orbital exposure (Liu & Abdala 2022). In *Moschorhinus*, the frontal makes a moderate contribution to the dorsal orbital wall as well, but its contact with the prefrontal appears very short in this taxon (Durand 1991: fig. 12) compared to what is observed in *Oliverosuchus* (Figs 2–4), *Euchambersia* (Liu & Abdala 2022), and (probably) *Promoschorhynchus* (Mendrez 1974; Huttenlocker *et al*. 2011).The ventral surface of the frontals of BP/1/3849 is characterized by a deep, elongated depression, which marks the location for the olfactory bulbs of the brain (Fig. 7). The lateral and partially the anterior limit

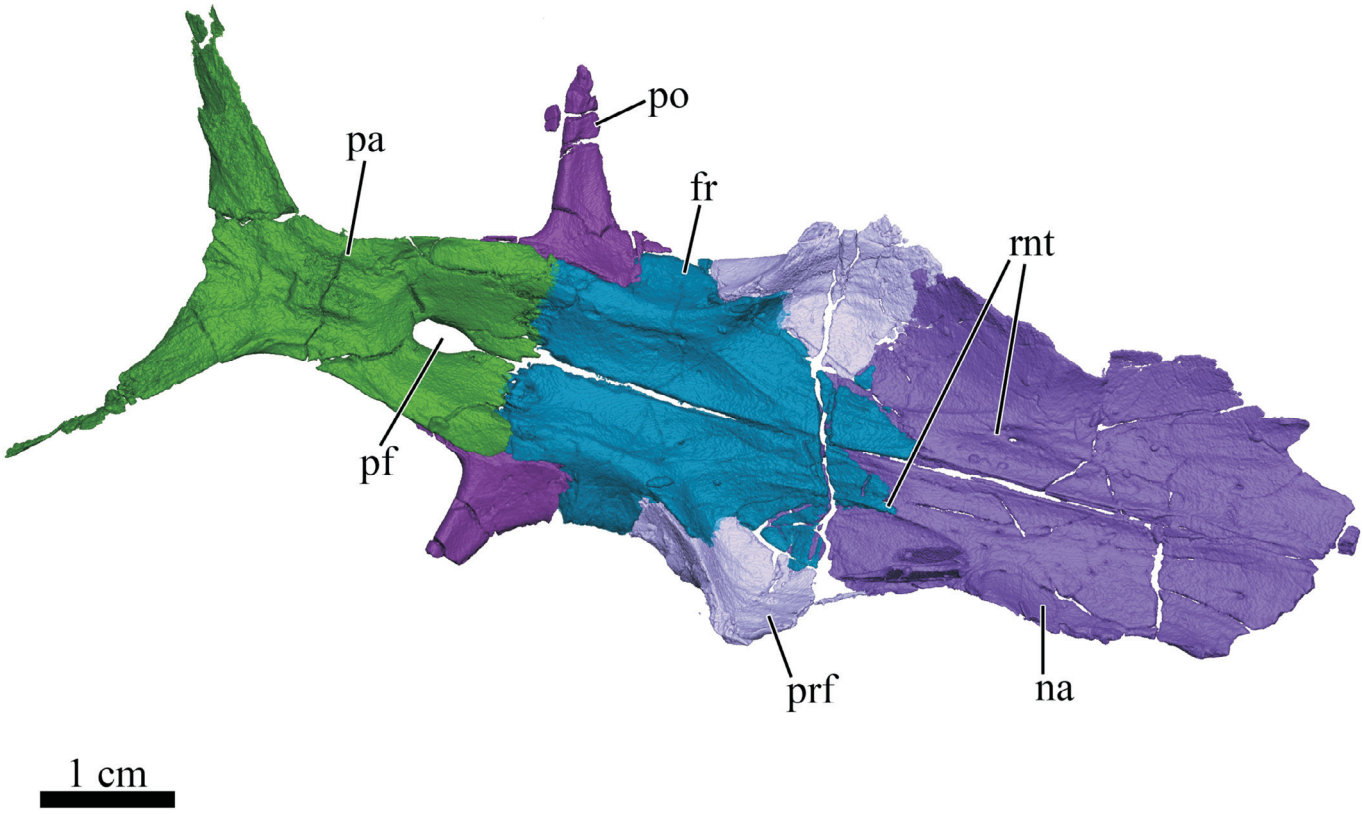


**Figure 7**. Three-dimensional reconstruction of the skull roof of BP/1/3849 in ventrolateral view. *Abbreviations*: fr, frontal; na, nasal; pa, parietal; pf, parietal foramen; po, postorbital; prf, prefrontal; rnt, ridges for cartilaginous nasal turbinals.

of the olfactory bulbs is bounded by two ridges running laterally to anteriorly, which partially separate them from the hindmost part of the nasal cavity. Comparable ridges have been described for the gorgonopsian *Cynariops* (Bendel *et al*. 2018), the basal cynodonts *Procynosuchus* (Kemp 1979), *Galesaurus* (Pusch *et al*. 2019), and *Bolotridon* (Pusch *et al*. 2021), and the probainognathian *Chiniquodon* (Kemp 2009). The posterior limit of the olfactory bulbs is not clearly visible, due to incomplete preservation of the frontals in that region, but is likely indicated by a gradual transition from slight concavity to convexity on the underside of the frontals at the level of the postorbital bar.

*Parietal*

The large parietals constitute the posterodorsal skull roof. Their lateral margins form the dorsal borders of the temporal fenestrae (Fig. 4). The parietal bone is anterolaterally overlapped by the posterior extensions of the postorbitals. Its anterior margin meets the frontal in an interdigitating suture and along its posteromedial margin the parietal contacts the postparietal (Figs 10, 12). The parietals are perforated in the midline by a large, oval parietal (= pineal) foramen (Figs 4, 7). Posterior to the parietal foramen, the parietals are fused. A distinct sagittal ridge extends posterior to the parietal foramen and continues posteriorly along the fused midline suture of the parietals before splitting to proceed onto the posterolateral processes of the parietals. Anteriorly, the ridge also splits, at the level of the parietal foramen, continuing as thin ridges on the dorsal surface of the postorbitals. The posterolateral processes of the parietals run parallel between the tabulars (which they overlap anteriorly) and the dorsomedial margins of the squamosals. Both processes are slightly damaged. The ventral margin of the parietal contacts the dorsal margin of the epipterygoid (Figs 3, 11). The ventral surface of the parietals is concave from its anterior margin to the level of the parietal foramen (Fig. 7). Posterior to the latter, the ventral surface of the parietals becomes convex. The surface texture of the parietals is smooth, comparable to that of the frontals.

*Postorbital*

The postorbital forms the posterodorsal dorsal edge of the orbit and the dorsal margin of the postorbital bar, with its anterior portion contacting the posterior portion of the frontal dorsolaterally, and overlies the anterolateral margin of the parietal with its posterior process (Figs 2–4). The descending process of the postorbital (only visible on the right side in the 3D reconstruction because of breakage on the left side) is a tapering, pointed structure.

**Palate**

*Vomer*

The vomer is an elongate, medially positioned element, extending anteroposteriorly and dividing the nasopharyngeal passage along the midline (Fig. 8). Its elongate interchoanal process expands anteriorly (as in all therocephalians) and constitutes roughly half of the length of the bone. It forms the medial border of the internal choanal opening, with maxillae forming the lateral borders.

The anterior portion of the vomer is somewhat crushed. As far as can be observed, the vomer extends anteriorly to

presumably overlie the vomerine process of the premaxilla, as in all akidnognathids (Huttenlocker 2009). Specimens of *Olivierosuchus* in which the vomer is better preserved (e.g. NMQR 3605; Botha-Brink & Modesto 2011) show that the anterior vomer is similar to that of *Promoschorhynchus* (Mendrez 1974), *Annatherapsidus* (Ivakhnenko 2011), *Shiguaignathus* (Liu & Abdala 2017), and *Jiufengia* (Liu & Abdala 2019), taking the form of an elongate isosceles triangle. By contrast, the anterior vomer of *Moschorhinus* is proportionally anteroposteriorly shorter and substantially more transversely expanded (Mendrez 1974; Durand 1991). No contact between the vomer and maxilla is present, unlike some whaitsiid and baurioid eutherocephalians (Hopson & Barghusen 1986). In *Olivierosuchus* and other akidnognathids, the interchoanal process of the vomer reaches its greatest expansion anterior to the canine at the point of contact with the vomerine process of the premaxilla, as also seen in e.g. the whaitsiid *Microwhaitsia* (Huttenlocker & Smith 2017) and the basal therocephalian *Lycosuchus* (Pusch *et al*. 2020). The interchoanal process of the vomer in BP/1/3849 is narrowest at the level of the posterior margin of the choanae, where it contacts the palatine, as in other akidnognathids.

The dorsal surface of the vomer of BP/1/3849 has a distinct median ridge, which extends posteriorly along the entire length of the interchoanal process and continues onto the anterior process of the pterygoid (Fig. 8A), comparable to what is observed in *Shiguaignathus* (Liu & Abdala 2017). The dorsal margin of this ridge has a slight median groove, which might have supported the ventral margin of a cartilaginous nasal septum, comparable to what has been described for basal therocephalians (van den Heever 1994; Pusch *et al*. 2020) and cynodonts (e.g. Fourie 1974; Crompton *et al*. 2015, 2017; Pusch *et al*. 2019). Unlike the basal therocephalian *Lycosuchus* (Pusch *et al*. 2020), in which the posterior portion of the vomer becomes a transversely broad, plate-like element at the level where it contributes to the posterior margin of the choana, the posterior portion of the vomer of BP/1/3849 only slightly expands here, comparable to the condition observed in other akidnognathids (e.g. Mendrez 1974; Durand 1991; Liu & Abdala 2017, 2019) and non-akidnognathid eutherocephalians such as the lycideopid *Tetracynodon* (Sigurdsen *et al*. 2012) and the whaitsiid *Theriognathus* (Huttenlocker & Abdala 2015). Immediately posterior to the internal choanae, the vomer of BP/1/3849 is laterally overlapped by the palatines and posteriorly by the anterior process of the pterygoid in dorsal view (Fig. 8A).

The ventral surface of the anterior process of the vomer is vaulted. However, this vaulted morphology is somewhat difficult to see in BP/1/3849 due to damage, and is more obvious in NMQR 3605. Posterior to the anterior vaulted portion, the vomer is keeled, bearing a ventromedian crest that extends from the interchoanal process onto the posterior portion of the vomer (Fig. 8B), as in other akidnognathids (e.g. Mendrez 1974; Durand 1991; Liu & Abdala 2017) and other eutherocephalians such as the whaitsiid *Theriognathus* (Huttenlocker & Abdala 2015). This differs from what has previously been described for *Olivierosuchus* based on the specimen NMQR 3605, in which a ventromedian crest seems to be only present on the posterior portion of the vomer (Botha-Brink & Modesto 2011; Liu & Abdala 2017, 2019). The vomer of the basal Chinese akidnognathid *Jiufengia* was described as lacking a ventromedian crest (Liu & Abdala 2019), but the bone surface in that specimen is poorly preserved, so it is uncertain whether the absence of this crest is biological or taphonomical.

*Palatine*

The palatine is a large bone that forms much of the palatal plate. It is situated between the vomer and the maxilla. In dorsal view, the palatine has three lateral processes. The first process is the anterolateral process, which extends anterolaterally to contact the maxilla (Figs 6C, 8A). The second process is the medial process, which rises highly dorsally to contact both the maxilla and the lacrimopalatine ridge. This process emerges out of an oblique ridge that terminates at an almost right angle to the long axis at the palatine-vomer suture in dorsal view. A comparable ridge is present in *Shiguaignathus* (Liu & Abdala 2017). This ridge of the palatine rises medially to form a distinct lamina on both sides in BP/1/3849 (Fig. 8A). These laminae resemble the medially directed plates of the palatines described for cynodonts, which form, together with the lateral wings of the vomer, a transverse lamina (Crompton *et al*. 2015, 2017; Pusch *et al*. 2019, 2021). However, unlike in cynodonts, the posterior portion of the vomer of BP/1/3849 does not have lateral 'wings', suggesting that the transverse lamina originated as a purely palatine structure in eutheriodonts prior to incorporating the vomer. The third process is the posterolateral process, which contacts the anterior process of the ectopterygoid posteriorly. This region also forms the anterolateral margin of the suborbital vacuity.

Posteromedially, the palatine contacts the anterior process of the pterygoid and forms the medial margin of the roughly circular suborbital vacuity. Anteriorly, the palatine forms the posterior margin of the internal choana. Laterally, the palatine bears the posterior portion of the crista choanalis, which is distinctly raised anteriorly, but becomes flatter posteriorly where it reaches the suborbital vacuity (Fig. 8B). The ventral morphology of the palatine of *Olivierosuchus* closely resembles that of *Promoschorhynchus* (Mendrez 1974), but differs from that of *Moschorhinus* (Durand 1991), in which this element is transversely broader and extends further anteriorly, making up nearly half of the lateral margin of the choana.

*Ectopterygoid*

The ectopterygoid is a slender bone, curved in ventral view, situated at the anterolateral edge of the transverse flange of the pterygoid and forming the lateral margin of the suborbital vacuity (Figs 6, 8). Posteromedially, it forms a thin plate overlapping the anterior face of the pterygoid transverse process. Anteriorly, it contacts the posterolateral process of the palatine, bearing a crest on its ventral edge extending from the crista choanalis. The anteriorly

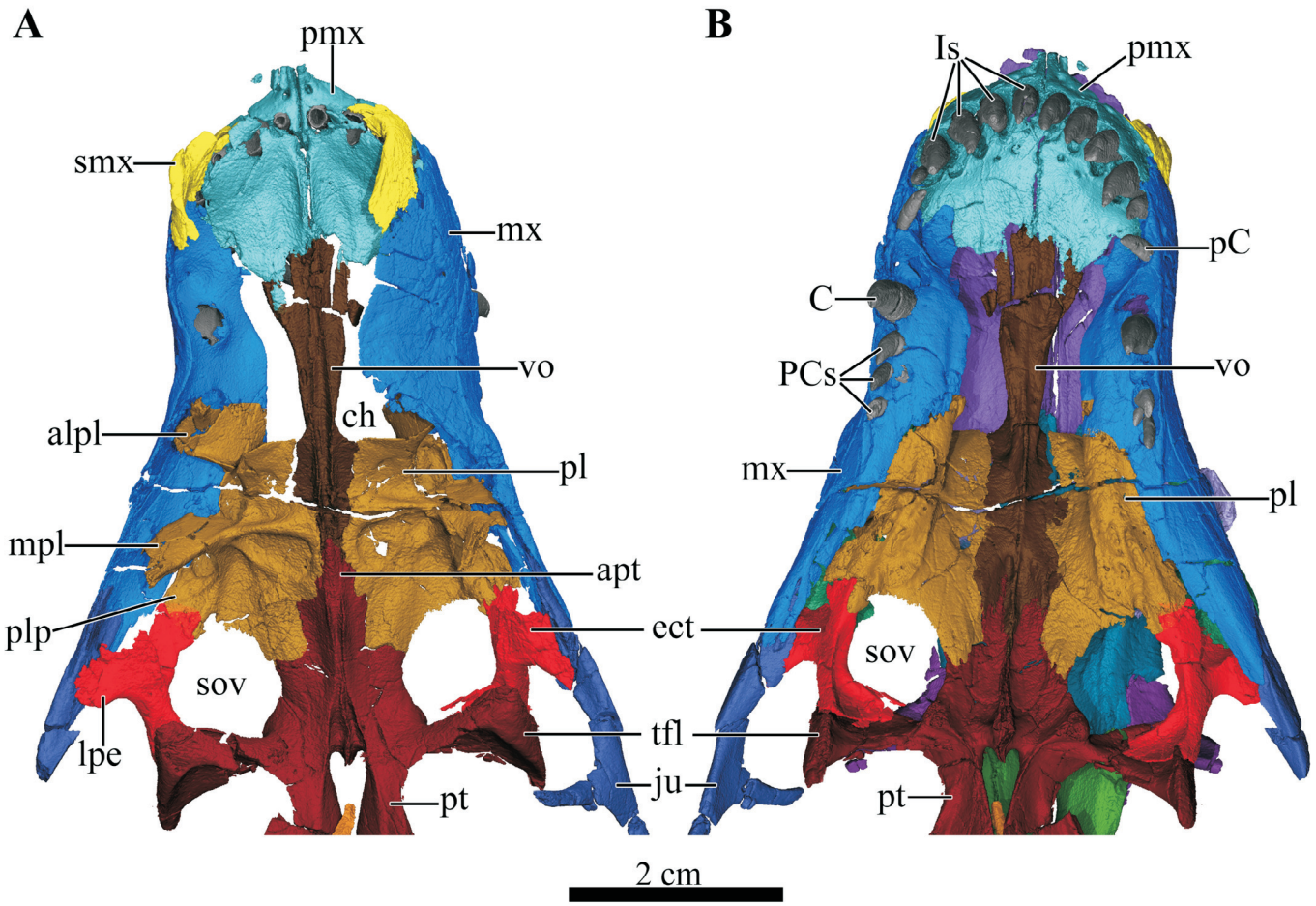


**Figure 8**. Three-dimensional reconstruction of the snout of BP/1/3849. **A**, dorsal view of the snout with the skull roof digitally removed to expose the internal structure; **B**, ventral view of the palate. *Abbreviation*s: alpl, anterolateral process of the palatine; apt, anterior process of the pterygoid; C, upper canine; ch, choana; ect, ectopterygoid; Is, upper incisors; ju, jugal; lpe, lateral process of the ectopterygoid; mpl, medial process of the palatine; mx, maxilla; pC, upper precanine; PCs, upper postcanines; pl, palatine; plp, posterolateral process of the palatine; pmx, premaxilla; pt, pterygoid; smx, septomaxilla; sov, suborbital vacuity; tfl, transverse flange of the pterygoid; vo, vomer.

canted dorsal portion of the ectopterygoid becomes confluent with the lacrimo-ectopterygoidal ridge of the lacrimal at its terminus (Figs 6, 10). In general, the ectopterygoid anatomy of *Olivierosuchus* is similar to that of other therocephalians. However, it differs from that of basal therocephalians such as *Alopecognathus* and *Lycosuchus* (van den Heever 1994; Pusch *et al*. 2020) in bearing a distinct lateral process of the ectopterygoid contacting the jugal, as has also been described for *Promoschorhynchus* (Mendrez 1974), *Tetracynodon* (Sigurdsen *et al*. 2012), and *Theriognathus* (Huttenlocker & Abdala 2015). However, the slender, laminar morphology of the former taxa differs from the broader, crescentic ectopterygoid of *Theriognathus*, in which the ectopterygoid broadly contacts the palatine and pterygoid medially based on the absence of a suborbital vacuity (Huttenlocker & Abdala 2015). It also differs from that of *Moschorhinus*, in which the ectopterygoid also appears broader and flatter (Durand 1991), albeit not crescentic as in *Theriognathus*.

*Pterygoid*

The pterygoid forms the posterior portion of the palate and parts of the basicranial girder (Figs 6, 8, 11). Its anterior process, which is situated between the suborbital vacuities, overlaps the posterior portion of the vomer in dorsal view and is bifurcated by the vomer in ventral view. A sharp ventromedial crest extends throughout the length of the anterior process, continuing onto the vomer. This crest widens at its posterior end, forming the rugose ventromedian process common to therocephalians (Huttenlocker 2009) immediately anterior to the heart-shaped interpterygoid vacuity. Two prominent, edentulous tuberosities are positioned lateral to the posterior portion of this crest and extend anterolaterally from the interpterygoid vacuity. The latter is posteriorly bisected by a relatively short cultriform process of the parasphenoid, which extends anteriorly for around half the length of the interpterygoid vacuity. In dorsal view, the median ridge of the vomer extends posteriorly along the anterior process of the pterygoid. This ridge tapers posteriorly and bifurcates, just anterior to the interpterygoid vacuity, into two ridges proceeding lateral to the latter (Fig. 8A). The posterior portion of the pterygoid contacts the basipterygoid articulation of the parasphenoid and makes up the floor of the braincase. Two long, slender, weakly curved quadrate processes extend posterolaterally to contact the quadrates (Fig. 11). In the anterior half of these processes, the pterygoid also extends medially as a thin, ventrally concave lamina underlying the parasphenoid.

**Braincase and occiput**

*Orbitosphenoid*

The paired orbitosphenoid (Fig. 9) is a seldom preserved

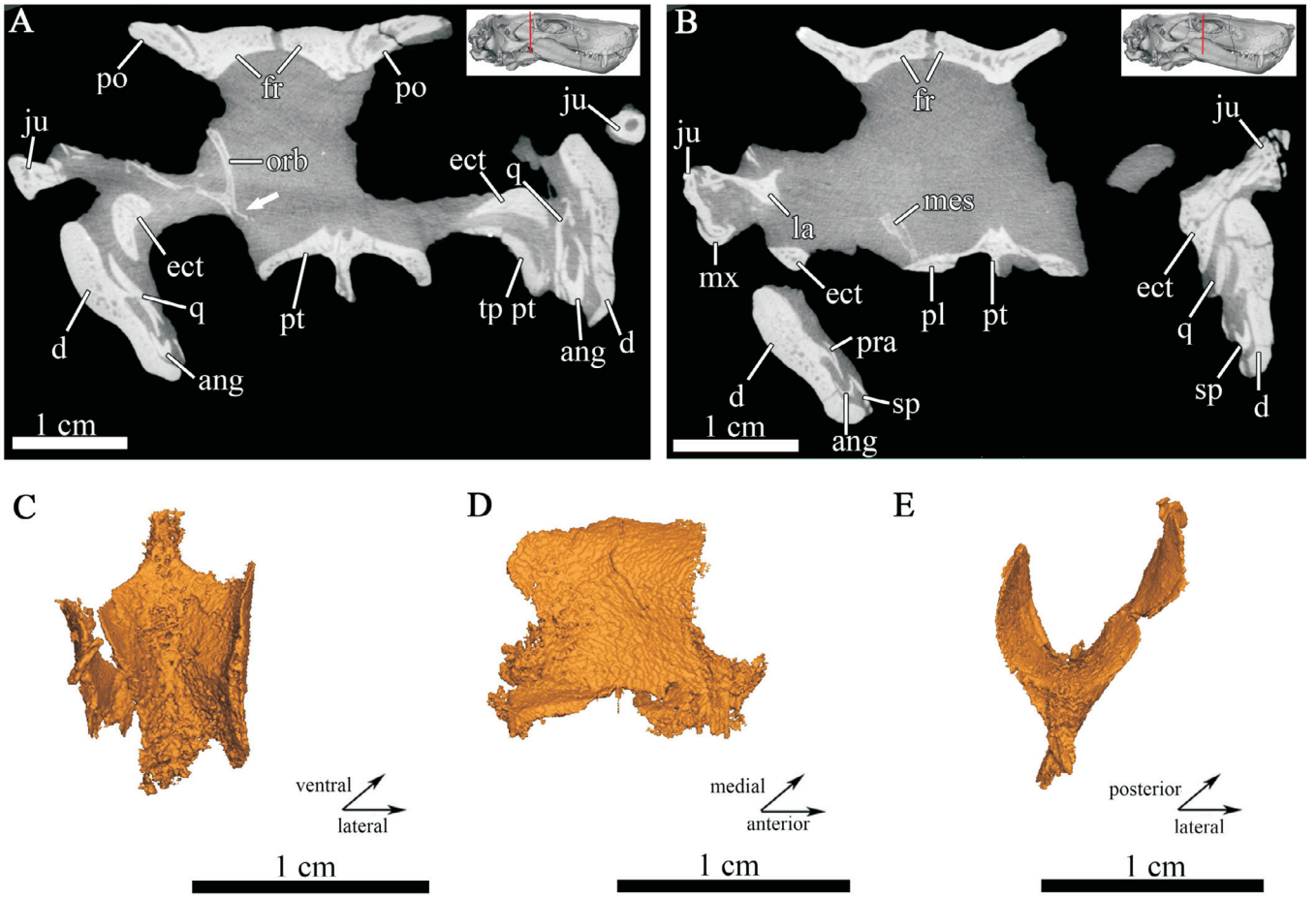


**Figure 9**. Transverse CT sections through the brain cavity in **A**, and **B**, of BP/1/3849. Reconstruction of the orbitosphenoid in **C**, dorsal view, **D**, lateral view, and **E**, anterior view. Arrow marks the position of the ventral keel of the orbitosphenoid. *Abbreviations*: ang, angular; d, dentary; ect, ectopterygoid; fr, frontal; ju, jugal; la, lacrimal; mes, mesethmoid; mx, maxilla; orb, orbitosphenoid; pl, palatine; po, postorbital; pra, prearticular; pt, pterygoid; q, quadrate; sp, splenial; tp pt, transverse process of the pterygoid.

endocranial bone, which typically loosely articulates with the frontal bones to build the ventral and partial lateral borders of the anterior braincase, supporting the olfactory bulbs of the brain in non-mammalian therapsids (Benoit *et al*. 2017a). In non-cynodont therapsids such as gorgonopsians (Benoit *et al*. 2017a) and the baurioid therocephalians *Tetracynodon* (Sigurdsen *et al*. 2012), *Microgomphodon* (Abdala *et al*. 2014), and *Mupashi* (Huttenlocker & Sidor 2016), the paired orbitosphenoids converge ventrally to form the ventromedian interorbital septum. This complex in BP/1/3849 was already figured in a CT-slice by Benoit *et al*. (2017a), but not described. In BP/1/3849, the orbitosphenoids have been displaced from their *in situ* position and have been strongly shifted to the left side of the skull, where they seem to 'float' between the postorbital bar dorsally and the pterygoid ventrally (Fig. 9A). The orbitosphenoids of *Olivierosuchus* consist of two plate-like structures, which are fused ventrally. The structure itself is indistinguishably fused to the mesethmoid anteriorly and the interorbital septum ventrally, with the entire complex forming a sphenethmoid element. In cross-section the sphenethmoid appears Y-shaped and thin, with a cancellous interior that is unusual for a non-cynodont therapsid. Unlike in the gorgonopsians sampled by Benoit *et al*. (2017a) and Bendel *et al*. (2018), in which the orbitosphenoids are fused ventrally into a long and hemi-cylindrical bone that encapsulates a tubular braincase, the orbitosphenoids of *Olivierosuchus* appear anteroposteriorly shorter and more closely resemble the cynodont condition.

*Epipterygoid*

The epipterygoid is a flat, blade-like, vertically oriented element situated dorsal to the quadrate process of the pterygoid and forming a partial sidewall of the braincase (Figs 3, 10). As previously described by Botha-Brink & Modesto (2011), the epipterygoid of *Olivierosuchus* appears slightly narrower than that of *Promoschorhynchus* (Huttenlocker *et al*. 2011) and is considerably narrower that in the whaitsiid *Theriognathus* (Barry 1965; Huttenlocker & Abdala, 2015), which is greatly expanded and resembles the morphology described for cynodonts. The anterior margin of the epipterygoid in BP/1/3849 is slightly concave and forms the posterior border of the orbital vacuity through which the ophthalmic branch ($V_1$) of the trigeminal nerve passed. Dorsally, its ascending process widens towards its contact with the parietal. The posterior margin of the bone forms the anterior border of a relatively large foramen through which the trigeminal nerve (V) passed (Fig. 10), but lacks a posterior apophysis. The ventral footplate shares only a short connection with the quadrate process of the pterygoid and extends towards, but does not contact, the prootic or the squamosal (Figs 4, 11).

*Prootic*

The prootic contributes to the sidewall of the braincase in front of the ear region and forms the anterior wall of the vestibule and the inner ear (Figs 10, 11, 12C). The pila antotica, an anterodorsally directed process of the prootic, lies medial to the epipterygoid and forms the lower border of the trigeminal foramen. The base of the pila antotica is broad and curves medially to overlap the posterolateral portion of the basisphenoid and the anteriormost tip of the basioccipital in dorsal view. This contrasts with what has been described for early cynodonts such as *Procynosuchus* (Kemp 1979), *Galesaurus* (Pusch *et al*. 2019), and likely also charassognathids (Huttenlocker & Sidor 2020), in which the pila antotica appears narrow and straight and only has a short contact with the posterolateral portion of the basisphenoid anteriorly, but shares a larger contact with the anterolateral margin of the basioccipital instead. A similar broad, medially curving morphology of the basal pila antotica has been described for *Lycosuchus* (Pusch *et al*. 2020), but in that taxon, the medial process of the prootic overlies most of the anterodorsolateral surface of the basioccipital. The prootic further exhibits a short anterodorsal process, which extends anteromedially and forms, together with the pila antotica, the 'incisure prootica' (Mendrez 1974), a moderately deep emargination that forms the posterior border of the trigeminal foramen (Fig. 11). Dorsally, the prootic contacts the supraoccipital, posteriorly the opisthotic, and with its posterodorsal process, which is only preserved on the left side, it contacts the squamosal. Together with the squamosal, the prootic slightly contributes to the anterior opening of the post-temporal fenestra (Fig. 12). The right prootic further preserves a short lateral flange at the base of its ventrolateral surface, which contacts a finger-like otic process on the anteromedial face of the squamosal to bound the pterygo-paroccipital foramen (Fig. 11B).

*Parabasisphenoid*

The fused parabasisphenoid forms the anterior floor of the braincase. It extends posteriorly from the basisphenoid process of the pterygoid, where its short cultriform process projects anteriorly between the pterygoids and bisects the interpterygoid vacuity (Fig. 11). Immediately before it contacts the pterygoid, the parasphenoid is pierced by a relatively large median foramen, from which a sharp ventromedian keel extends posteriorly along the ventral surface of the parabasisphenoid, as in other therocephalians. Posteriorly, the parabasisphenoid flares out into two divided tuberosities, the tubercula spheno-

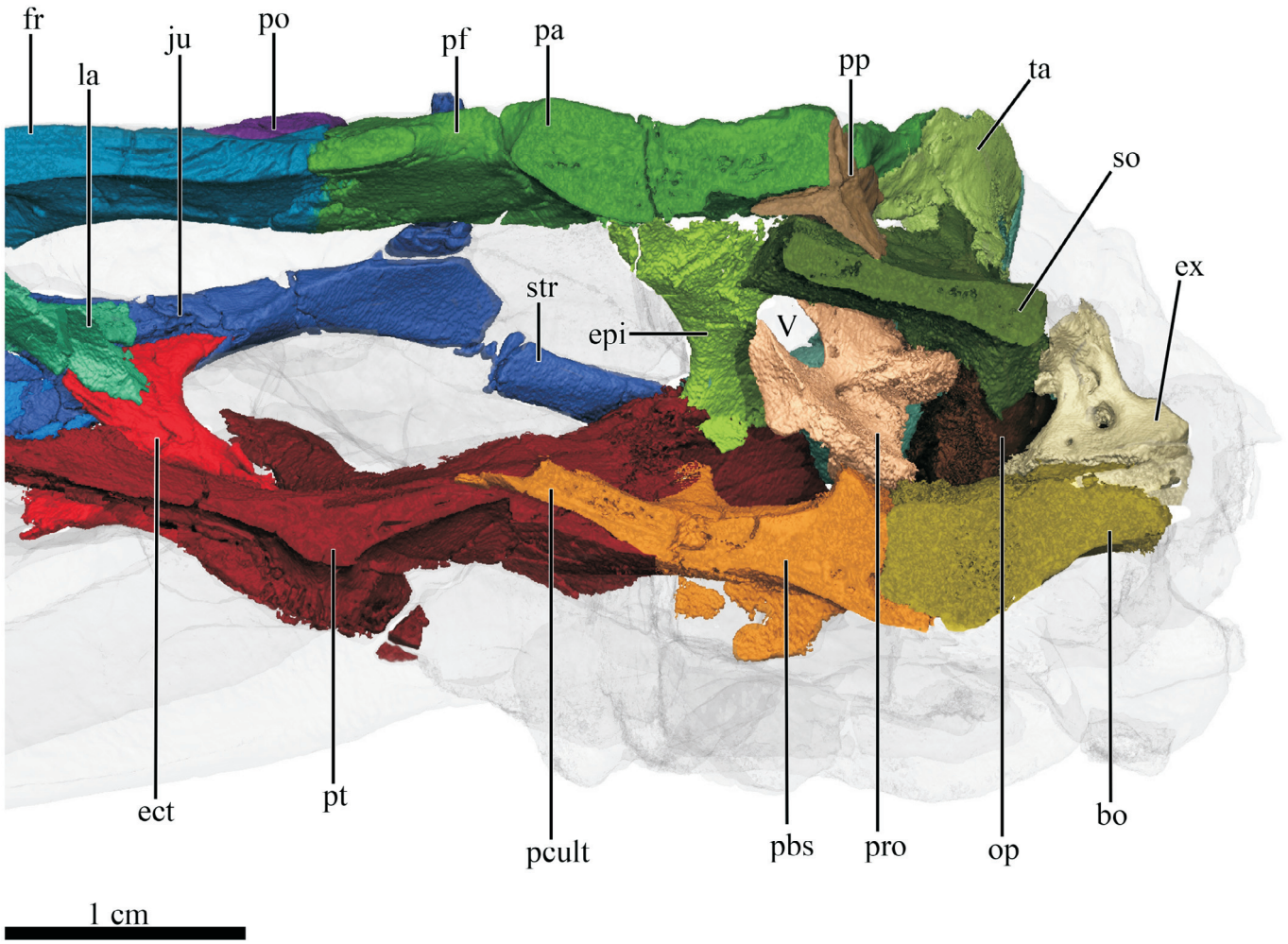


**Figure 10**. Mid-sagittal section through the reconstructed braincase of BP/1/3849. *Abbreviations*: bo, basioccipital;ect, ectopterygoid; epi, epipterygoid; ex, exoccipital; fr, frontal; ju, jugal; la, lacrimal; op, opisthotic; pa, parietal; pbs, parabasisphenoid; pcult, cultriform process of the parasphenoid; pf, parietal foramen; po, postorbital; pp, postparietal; pro, prootic; pt, pterygoid; so, supraoccipital; str, subtemporal ramus of the jugal; ta, tabular; V, trigeminal nerve opening.

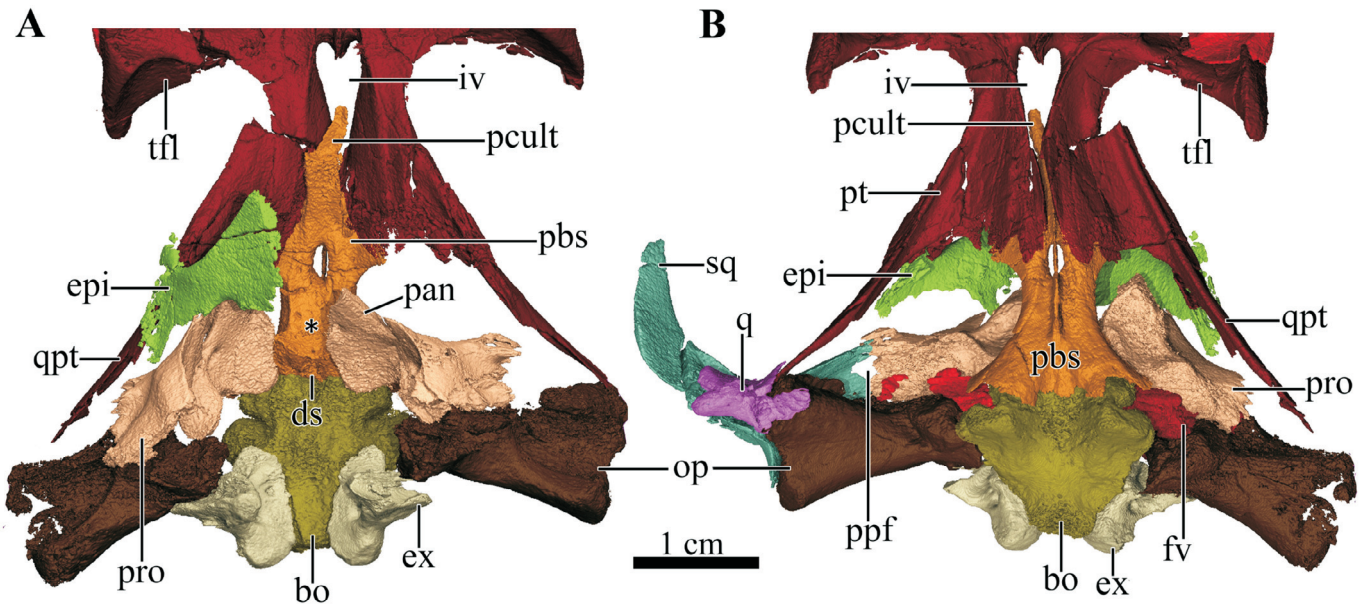


**Figure 11**. Three-dimensional reconstruction of the floor of the braincase of BP/1/3849 in **A**, dorsal and **B**, ventral view. The right epipterygoid was digitally removed in **A**, and the left squamosal and quadrate in **B**. Asterisk indicates the location of the sella turcica in **A**. *Abbreviations*: bo, basioccipital; ds, dorsum sellae; epi, epipterygoid; ex, exoccipital; fv, fenestra vestibuli; iv, interpterygoid vacuity; op, opisthotic; pbs, parabasisphenoid; pcult, cultriform process of the parasphenoid; ppf, pterygoparoccipital foramen; pan, pila antotica; pro, prootic; pt, pterygoid; q, quadrate; qpt; quadrate process of the pterygoid; sq, squamosal; tfl, transverse flange of the pterygoid.

occipitale or basal tubera, leaving a deep trough between them. The parabasisphenoid contacts the basioccipital posteriorly in a relatively straight suture. The basisphenoid wing (or parasphenoid ala) is relatively short and contributes to the anterior margin of the fenestra vestibuli (Fig. 11B). In dorsal view (Fig. 11A), the basisphenoid meets the paired bases of the pilae antoticae of the prootics, by which it is strongly overlapped posterolaterally, in front of an unossified space, the 'unossified zone' of Olson (1994). A small dorsum sellae occupies the posteriormost end of the parabasisphenoid in front of the unossified zone. This structure is flanked by the bases of the pilae antoticae and marks the posterior end of the sella turcica, a shallow depression on the dorsal surface of the parabasisphenoid, which indicates the position of the hypophysis.

*Basioccipital*

The basioccipital forms the posterior floor of the braincase, part of the occipital condyle, and ventral part of the occiput. Its dorsal surface is marked by a pronounced depression, which forms the floor of the hindbrain (cerebellum) region. Anteriorly, its dorsal surface is slightly overlain by the paired bases of the pilae antoticae of the prootics (Fig. 11A). Laterally, it contacts the opisthotic and posterolaterally its dorsal surface is overlain by the exoccipital (Figs 11, 12). The jugular foramen housing cranial nerves IX, X, and XI faces ventrally and is medially bordered by the basioccipital and exoccipital and laterally by the opisthotic. In ventral view, the anterolateral surface of the basioccipital has a prominent lateral boss, its contribution to the basal tuber, on either side. In this area, the basioccipital contributes to the medial wall of the fenestra vestibuli (Fig. 11B).

*Opisthotic*

The opisthotic contributes to the posterolateral border of the braincase and forms the wide, transversely oriented paroccipital process (Figs 11, 12). The paroccipital process is dorsoventrally constricted at its base and extends ventrolaterally to articulate with the squamosal. Together, the squamosal and opisthotic enclose the post-temporal fenestra, as in other akidnognathids such as *Promoschorhynchus* (Mendrez 1974; Huttenlocker *et al*. 2011), *Moschorhinus* (Durand 1991), *Jiufengia* (Liu & Abdala 2017), and *Euchambersia* (Liu & Abdala 2019) and various non-akidnognathid therocephalians such as *Lycosuchus* (van den Heever 1994) and *Theriognathus* (Huttenlocker & Abdala 2015). In posterior view, the post-temporal fenestra is bounded dorsally and medially by the posterodorsal process of the opisthotic, which contacts the supraoccipital dorsally and the exoccipital medially, and by the paroccipital process of the opisthotic ventrally (Fig. 12B,D). As in all therocephalians, the paroccipital process bears a shallow depression on its dorsal surface in the floor of the post-temporal fenestra. The mastoid process of the opisthotic extends posterolaterally from the paroccipital process and reaches anteriorly, where its concave lateral margin lies in a medially facing fossa of the squamosal and makes additional contact with the quadrate. A short but robust ventromedial process of the opisthotic contacts the posterolateral margin of the basioccipital. Anteriorly, it contacts the prootic and forms the posterior border of the fenestra vestibuli and the inner ear.

*Supraoccipital*

The supraoccipital is a plate-like, median, transversely broad and dorsoventrally narrow bone, which forms the

dorsal border of the foramen magnum (Fig. 12). In occipital view, the bone is bordered by the postparietal dorsally, the tabulars and the squamosals laterally, and the opisthotics and exoccipitals ventrolaterally. The contact between the supraoccipital and the squamosal is only present on the left side of the skull due to damage of the right squamosal. The supraoccipital is strongly inclined anterodorsally to posteroventrally in BP/1/3849 due to compression of the dorsal occipital plate (Fig. 10). Anteriorly, the supraoccipital forms a distinct wedge, which underlies the prootic ventrally, the postparietal dorsally and sutures the dorsalmost portion of the ascending process of the epipterygoid in internal view, comparable to what has been described for *Moschorhinus* (Durand 1991), *Theriognathus* (Huttenlocker & Abdala 2015), and *Mupashi* (Huttenlocker & Sidor 2016). A possible anterior process of the supraoccipital, which underlies the postparietal dorsally, the prootic ventrally, and contacts the dorsalmost portion of the ascending process of the epipterygoid, seems to also be present in *Promoschorhynchus* (Mendrez 1974). The internal surface of the supraoccipital of BP/1/3439 is concave and forms the roof of the hindbrain (cerebellum) region (Fig. 12C).

*Exoccipital*

The exoccipitals are paired, triradiate bones that frame the foramen magnum laterally on the occipital plate and contribute to the occipital condyle (Fig. 12). Their clubbed ventral processes contact the posterolateral portion of the basioccipital and form the dorsomedial margin of the jugular foramen. The exoccipital has an expanded dorsal process contacting the posterodorsal process of the opisthotic laterally and the supraoccipital dorsally (Figs 11, 12). They bear a medial tubercle on each side for articulation with the proatlas. However, the proatlas in this specimen is not preserved, only the left atlas neural arch and the possible broken anterolateral edge of the atlas pleurocentrum articulate with the exoccipital on the left side (Fig. 12B).

*Postparietal*

The postparietal is a flat, vertically oriented, median

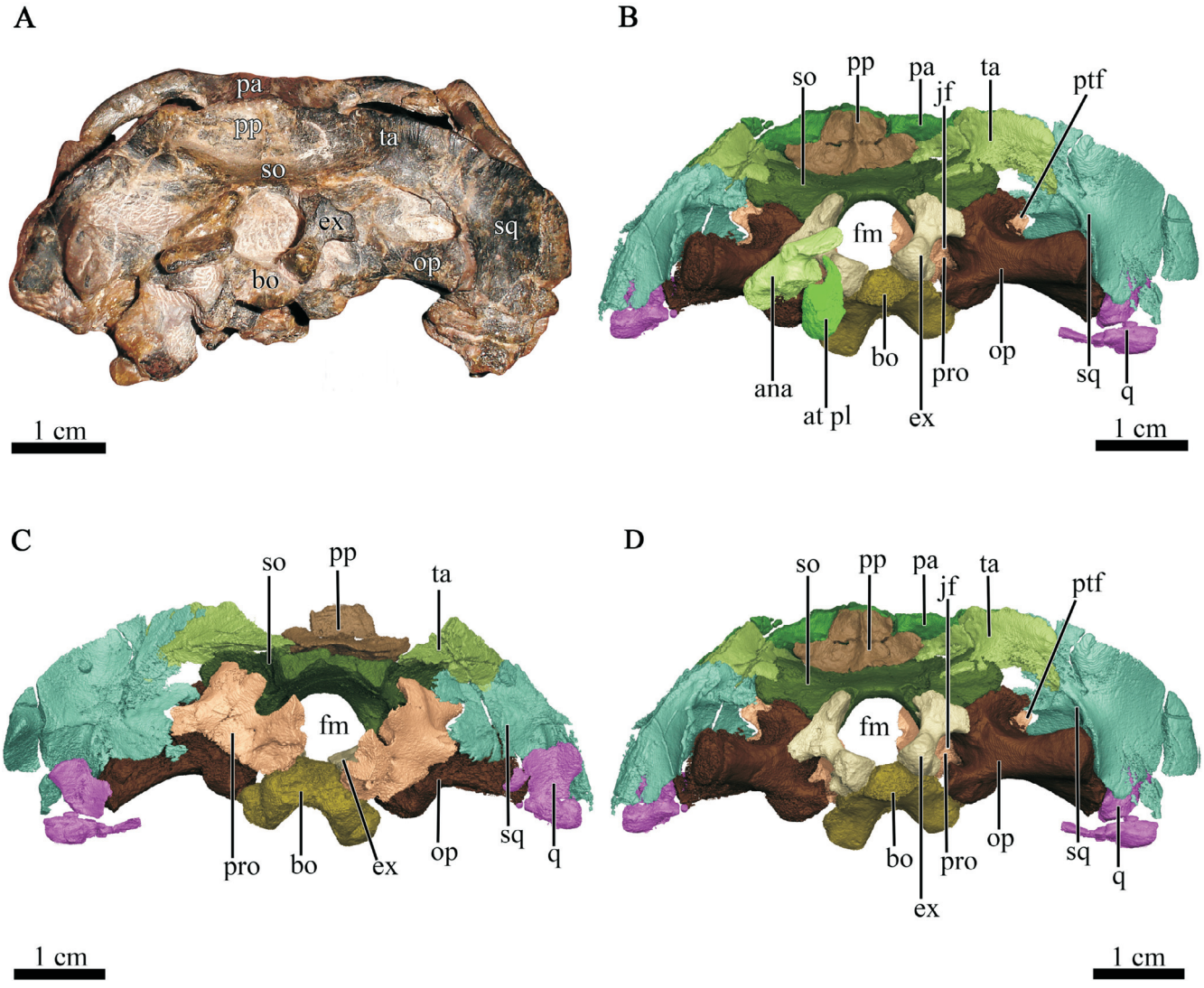


**Figure 12**. Occiput of BP/1/3849. **A**, photograph of the skull in posterior view. **B**, posterior view of the 3D reconstructed occiput including articulated postcranial bones. **C**, 3D reconstruction of the braincase in anterior view with the parietal digitally removed. **D**, Posterior view of the 3D reconstructed occiput. *Abbreviations*: ana, atlantal neural arch; at pl, atlas pleurocentrum; bo, basioccipital; ex, exoccipital; fm, foramen magnum; jf, jugular foramen; op, opisthotic; pa, parietal; pp, postparietal; pro, prootic; ptf, posttemporal fenestra; q, quadrate; so, supraoccipital; sq, squamosal; ta, tabular.

wing-shaped bone that forms much of the dorsal occipital surface. It is bordered dorsally and dorsolaterally by the parietal, laterally by the paired tabulars, and ventrally by the supraoccipital (Fig. 12). In occipital view, it bears a slight vertical crest (nuchal line) along its midline, which continues weakly onto the supraoccipital. As in other therocephalians, the postparietal is wider than tall. Dorsal to its lateral 'wings', a portion of the parietal makes contribution to the dorsal occipital surface. The postparietal has a relatively long anterior flange, which shares a sutural connection to the underside of the posterior portion of the parietal (Fig. 10). Together with the parietal and the supraoccipital below, the postparietal borders an unossified zone, which is poorly preserved in BP/1/3849 due to compression of the dorsal occipital plate.

*Tabular*

The paired tabulars are slender bones situated at the dorsolateral margins of the occiput (Fig. 4). They overlap the laminar temporal portions of the parietals and squamosals posteriorly. Unlike what has been described for *Moschorhinus* (Durand 1991), in which the dorsal process of the squamosal is fused to the tabular along most of its posterior surface, the squamosal and the tabular of *Olivierosuchus* are distinct from each other. Dorsally, the tabular of BP/1/3849 is bordered by the long posterolateral process of the parietal. It further bears a medial process contacting the postparietal laterally, and ventromedially, it slightly overlaps the lateral margin of the supraoccipital. Though the ventral margin of both tabulars is slightly damaged, it appears that they are somewhat restricted and neither contact the opisthotic ventrally nor extend around or below the post-temporal fenestra (Fig. 12).

*Squamosal*

The squamosal forms the dorsal margin of the posterior zygomatic arch and much of the posterolateral portion of the temporal region (Figs 2, 4). It is strongly curved and has a tall dorsomedial lamina covering the anterior face of the tabular laterally and also partially the posterolateral process of the parietal. This is most clearly visible on the left side of the skull, as the dorsomedial lamina of the right squamosal is not completely preserved. Ventrally, the medial lamina of the squamosal overlaps the dorsal and lateral portions of the paroccipital process of the opisthotic. The zygomatic process of the squamosal, which is only preserved on the right side, tapers steeply along its sutural contact with the posterior portion of the jugal (Fig. 2). Its anteroventral surface bears the quadrate recess accommodating the quadrate, which is preserved on both sides of the skull. Posterodorsally, the squamosal slightly contacts the lateral margin of the supraoccipital and the posterodorsal process of the prootic, which is only preserved on the left side due to damage of the right squamosal in that area. In occipital view, the squamosal and opisthotic enclose the post-temporal fenestra (Fig. 12B,D). Anteroventrally, the right squamosal has a finger-like otic process, which originates medial to the quadrate recess and quadrate process of the pterygoid and contacts the lateral flange of the prootic to bound the pterygo-paroccipital foramen (Fig. 11B).

**Lower jaw**

*Dentary*

The horizontal, tooth-bearing ramus of the dentary is fairly slender and tapers anteriorly towards the symphysis (Fig. 13). The lateral surface of the dentary is generally smooth, though it is marked by several cracks (Figs 2, 3, 13A). In lateral view, the dentary gently curves upwards at the symphysis, as in *Promoschorhynchus* (Mendrez 1974), but unlike some other akidnognathids such as *Moschorhinus*, *Euchambersia*, and *Jiufengia* (Durand 1991; Liu & Abdala 2019, 2022), in which the dentaries steeply curve upwards at the symphysis and form a distinct 'chin'. At the level of the symphysis, the lateral surface of the dentary in BP/1/3849 is slightly pitted with fine vascular foramina, which decrease in number towards the last lower postcanine. The dentaries are unfused at the symphysis and slightly dislocated where they have been shifted somewhat along the anteroposterior axis (Fig. 3). Posteriorly, the horizontal ramus of the dentary curves dorsally to form a high, almost rectangular coronoid process. The latter exhibits an elongated, shallow masseteric fossa on its lateral surface located just anterior to the mandibular fenestra. This fossa extends roughly halfway down the length of the horizontal ramus.

*Splenial*

The splenial is a thin, elongated element extending anteroposteriorly along the medial surface of the horizontal ramus of the dentary, by which it is completely obscured from lateral view. The splenial proceeds along an anteroposterior groove in the ventromedial surface of the dentary, the Meckelian groove, which would have housed the Meckelian cartilage in life. Anteriorly, it extends from a level where it contributes to the mandibular symphysis to a level near the posterior margin of the horizontal ramus of the dentary where it overlaps the anterior tip of the angular and contacts the prearticular dorsally (Fig. 13B,C).

*Angular*

The angular is a broad, vertically oriented plate which tapers anteriorly, where it rests medial to the posteroventral margin of the dentary and forms the ventral border of the mandibular fenestra. It runs lateral to the prearticular by which it is slightly overlain in medial view (Fig. 13B). The expanded reflected lamina, which is slightly damaged on both sides, covers the posterior end of the angular. The lateral surface of the reflected lamina bears four ridges separated by three depressions, the usual morphology for therocephalians (Olroyd & Sidor 2021). Three of these ridges taper outwards from their point of origin in the middle of the lamina, but the posteriorly-directed ridge becomes greatly expanded at its outer terminus (Figs 2, 13A). Medially, both the angular and the overlying prearticular are overlapped by the coronoid for a short span anterior to the mandibular

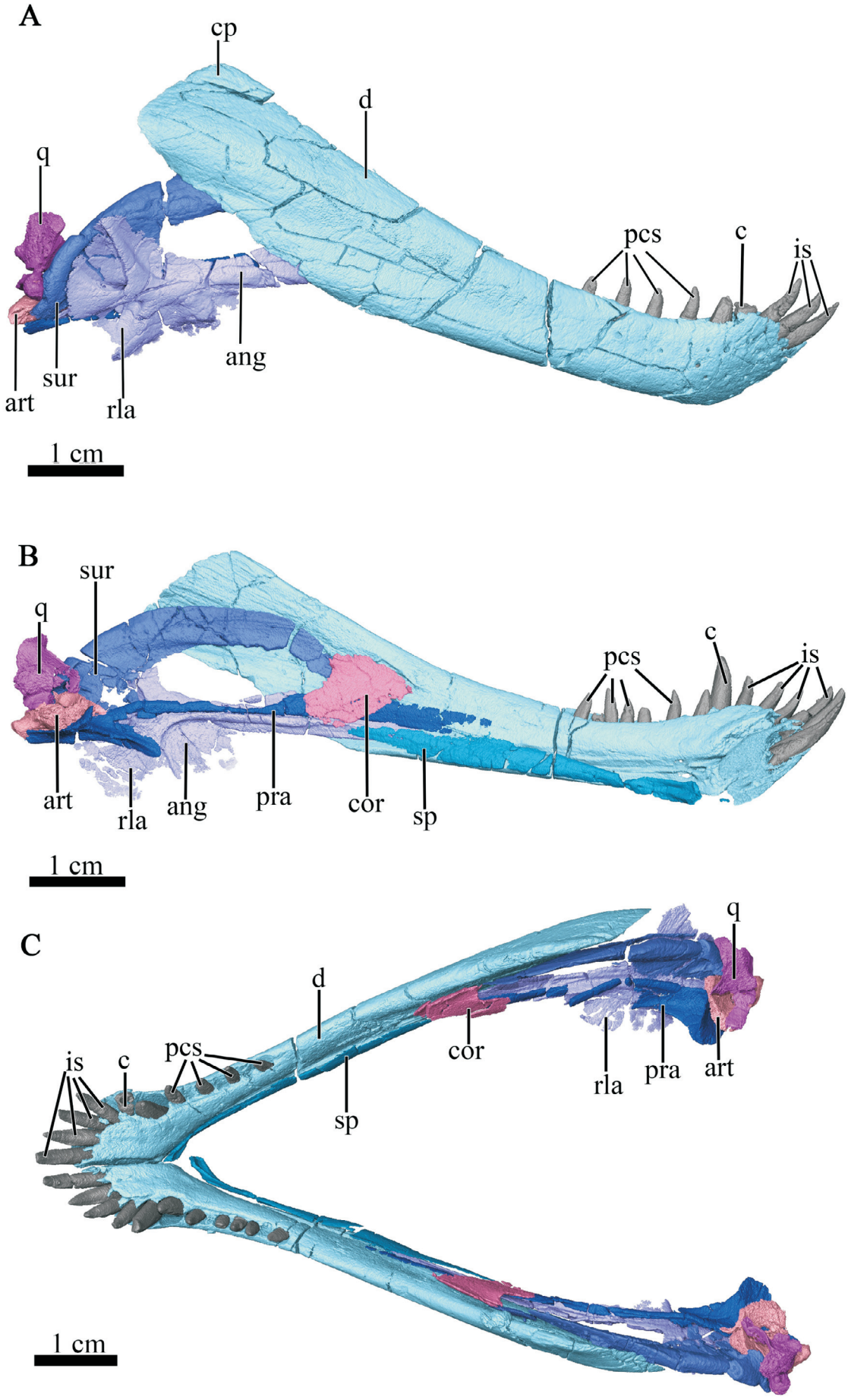


**Figure 13**. Three-dimensional reconstrcution of the right mandible of BP/1/3849 in **A**, lateral, **B**, medial, and **C**, dorsal view. *Abbreviations*: ang, angular; art, articular; c, lower canine; cor, coronoid; cp, coronoid process; d, dentary; is, lower incisors; pcs, lower postcanines; pra, prearticular; q, quadrate; rla, reflected lamina of the angular; sp, splenial; sur, surangular.

fenestra. In lateral view, the angular obscures most of the surangular, which rests against the posterodorsal corner of the angular.

*Surangular*

The surangular is a flat, arcuate bone that arches posterior and medial to the coronoid process and forms the dorsal border of the mandibular fenestra (Fig. 13). Anterior to this fenestra it curves downwards to underlie the coronoid. It is situated against the posterior portion of the angular. In this region, it further contacts the prearticular ventrally, and with its posteriormost end the quadrate and articular. Its posterolateral edge bulges out in a thin exposure between the angular and articular.

*Coronoid*

The coronoid is a thin, plate-like bone that lies medially to the dentary, just anterior to the coronoid process, and overlies the anterior portions of the prearticular and angular (Fig. 13B,C). It is roughly quadrilateral in shape and angled posteroventral to anterodorsally, with its anterodorsal edge being broader than its posteroventral extent. The posterior margin of the coronoid is weakly concave, and overlaps the anterior tip of the surangular medially. The posteroventral and anterodorsal edges of the coronoid are slightly out-of-plane with each other, with the former being more medial (Fig. 13C).

*Prearticular*

The prearticular is an anteroposteriorly elongated, rod-like element, which rests on an elongate medial shelf of the angular and forms the floor of the mandibular fenestra (Fig. 13B). Anteriorly it is a nearly vertical, ribbon-like element, but it curves inward and becomes more horizontal posteriorly. At its posterior tip, the prearticular bears a short medial process that underlies the articular (Fig. 13C).

*Articular*

The articular is a low, short bone that represents the posteriormost edge of the lower jaw (Fig. 13). It overlies the posteromedial process of the prearticular and contacts the quadrate dorsally and the surangular anteriorly. In their description of specimen NMQR 62, Botha-Brink & Modesto (2011) noted that the articular of *Olivierosuchus* bears a short retroarticular process. This cannot be confirmed in BP/1/3849 due to poor preservation, but we concur with its presence in NMQR 62 (Fig. 1G).

**Dentition**

Almost all teeth in both the upper and lower jaw are well preserved, except for the right lower canine, which is missing its crown. They are almost exclusively preserved in place, except for the first upper postcanine in the left maxilla and the fourth right lower postcanine, which have fallen out. Serrations are absent on both the distal and mesial margins of all teeth.

BP/1/3849 has five upper and four lower incisors, a conserved number in akidnognathids (Huttenlocker 2009). They are simple, conical and slightly recurved teeth that vary in size (Figs 1–6, 13). The upper incisors increase in size from I1 to I4, with the first and the second tooth being roughly similar in size, while the third and fourth upper incisors are considerably larger than I1 and I2. The fifth upper incisor in turn is markedly smaller than its predecessors (Figs 6B, 14A), as in most akidnognathids (e.g. Mendrez 1974; Durand 1991; Liu & Abdala 2017, 2019). By contrast, in the aberrant akidnognathid *Euchambersia*, the upper incisors increase in size from I1 to I5, with the I5 being only slightly smaller than the upper canine (Benoit *et al*. 2017c; Liu & Abdala 2022). Unlike the upper incisors, the lower incisors only slightly decrease in size from the first to fourth tooth in BP/1/3849 (Figs 13, 15). There are developing replacement teeth for upper incisors one and three in both premaxillae, and for the fifth incisor in the right premaxilla, which are located posterior to the functional tooth (Fig. 14B). There is a coalescence between the alveoli of the functional and replacement teeth of the left and right I3 and the right I5, with the replacements for the left I3 and the right I5 penetrating the root of the functional tooth, and the replacement for the right I3 eroding the root of the functional tooth. In the mandible, there are replacement teeth for the third lower incisors on both sides and for the first lower incisor in the right dentary, which are all still incipient and positioned posterior to the functional tooth (Fig. 15B). There is a coalescence visible between the alveoli of the functional and replacement teeth, with the replacement teeth for the left and right i3 and the right i1 slightly eroding the roots of their functional counterparts.

Each maxilla bears one precanine, one canine and three postcanines, with the first upper left postcanine having fallen out (Figs 8B, 14A). Both functional upper canines are in their posterior alveoli, with replacement canines visible in the CT data developing in the anterior alveoli. The functional canines are large and slightly recurved. On the left side, the unerupted replacement canine starts to erode the root of the functional canine anteriorly (Fig. 14B). *Olivierosuchus* has a relatively low maxillary postcanine count for an akidnognathid, with higher numbers present in *Promoschorynchus* (five; Mendrez 1974), *Shiguaignathus* (eight; Liu & Abdala 2017), and *Jiufengia* (four; Liu & Abdala 2017). However, this count exceeds that of *Euchambersia*, which lacks upper and lower postcanines entirely (Benoit *et al*. 2017c; Liu & Abdala 2022), and matches that of *Moschorhinus* (Durand 1991).

In each dentary there are five postcanine tooth positions, with the fourth lower postcanine in the right dentary having fallen out (Fig. 13). This differs slightly from what has been described for *Promoschorhynchus*, with six postcanines in each dentary (Mendrez 1974). The upper and lower postcanines are simple, conical teeth, with the uppers larger than the lowers. The upper third postcanines on both sides are considerably smaller than their predecessors.

There is a coalescence between the alveoli for the functional and replacement tooth of the left and right precanine, with the new precanine penetrating the root of the functional precanine (Fig. 14B). *Olivierosuchus* shows the usual alternating replacement of the upper canines

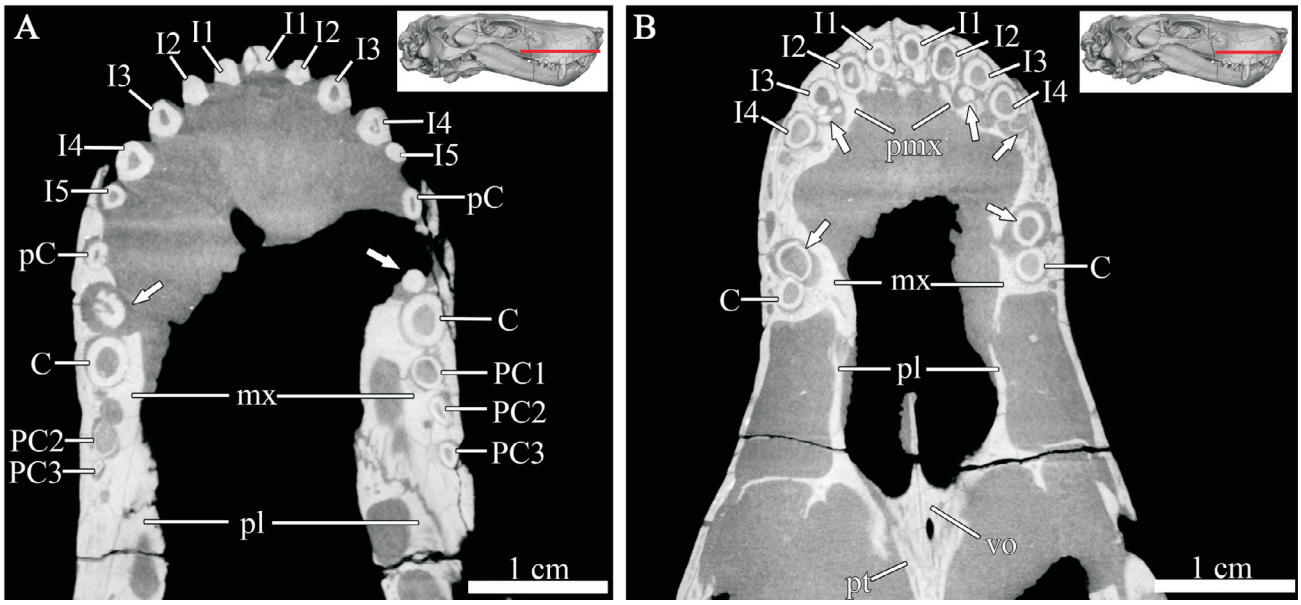


**Figure 14**. Horizontal CT sections through the upper jaw of BP/1/3849. Arrows mark the positions of replacement teeth in **A** and **B**. *Abbreviations*: C, upper canine; I, upper incisor; mx, maxilla; PC, upper postcanines; pC, upper precanines; pl, palatine; pmx, premaxilla; pt, pterygoid; vo, vomer.

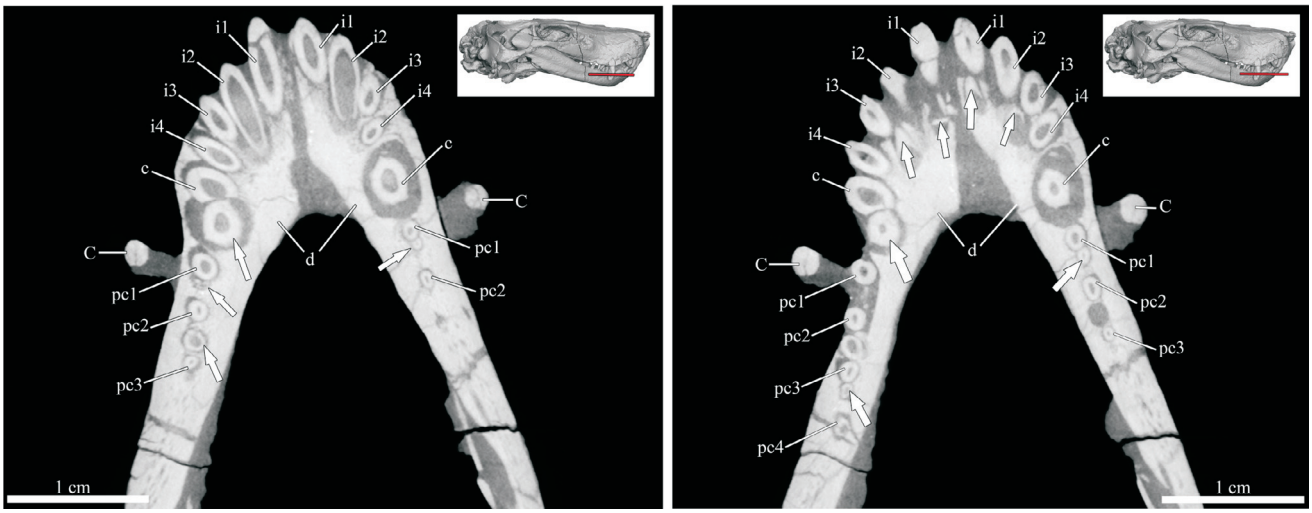


**Figure 15**. Horizontal CT sections through the lower jaw of BP/1/3849. Arrows mark the positions of replacement teeth. *Abbreviations*: C, upper canine; c, lower canine; d, dentary; i, lower incisor; pc, lower postcanine.

typical of non-mammalian theriodonts (Luo *et al*. 2004), with the persistent presence of two alveoli for the functional and replacement tooth. In each dentary, the replacement teeth for the canines do not occupy persistent separate alveoli and form posterior to the functional canine, as for the non-canine tooth positions. In BP/1/3849, they are penetrating the root of the functional canine and are already partially erupted (Fig. 15). There are no replacement teeth for upper postcanines visible in the CT data. Replacement teeth can be observed for lower postcanine one on both sides, and for the lower fourth postcanines on the left and the lower third postcanine on the right side, which are located posterior to the functional tooth.

## Ear region

*Quadrate*

The quadrate bone is situated at the posterolateral portion of the occiput. It consists of a dorsal plate and the ventral trochlea, the usual condition in therapsids (Luo & Crompton 1994; Pusch *et al*. 2019). In the right quadrate, both components appear disarticulated from another (Fig. 13A). The left quadrate is exposed in lateral view due to an incomplete squamosal in that region (Fig. 3). The ventral trochlea is broad, as in all therocephalians (Botha-Brink & Modesto 2011), and its ventral surface articulates with the dorsal margin of the articular bone of the mandible to form the jaw joint. The dorsal plate fits between the ventrolateral margin of the squamosal posteriorly and the lateralmost margin of the mastoid process of the opisthotic medially. The quadrate process of the pterygoid extends towards the anterior margin of the quadrate and medially contacts a thin lamina extending anteriorly from the ventral trochlea (visible on the right side of the skull, but damaged on the left; Fig. 11B). Laterally, the dorsal plate and trochlea of the quadrate are somewhat separated by a notch (the lateral notch). The quadratojugals do not appear to be preserved; these are small, columnar elements in therocephalians (van den

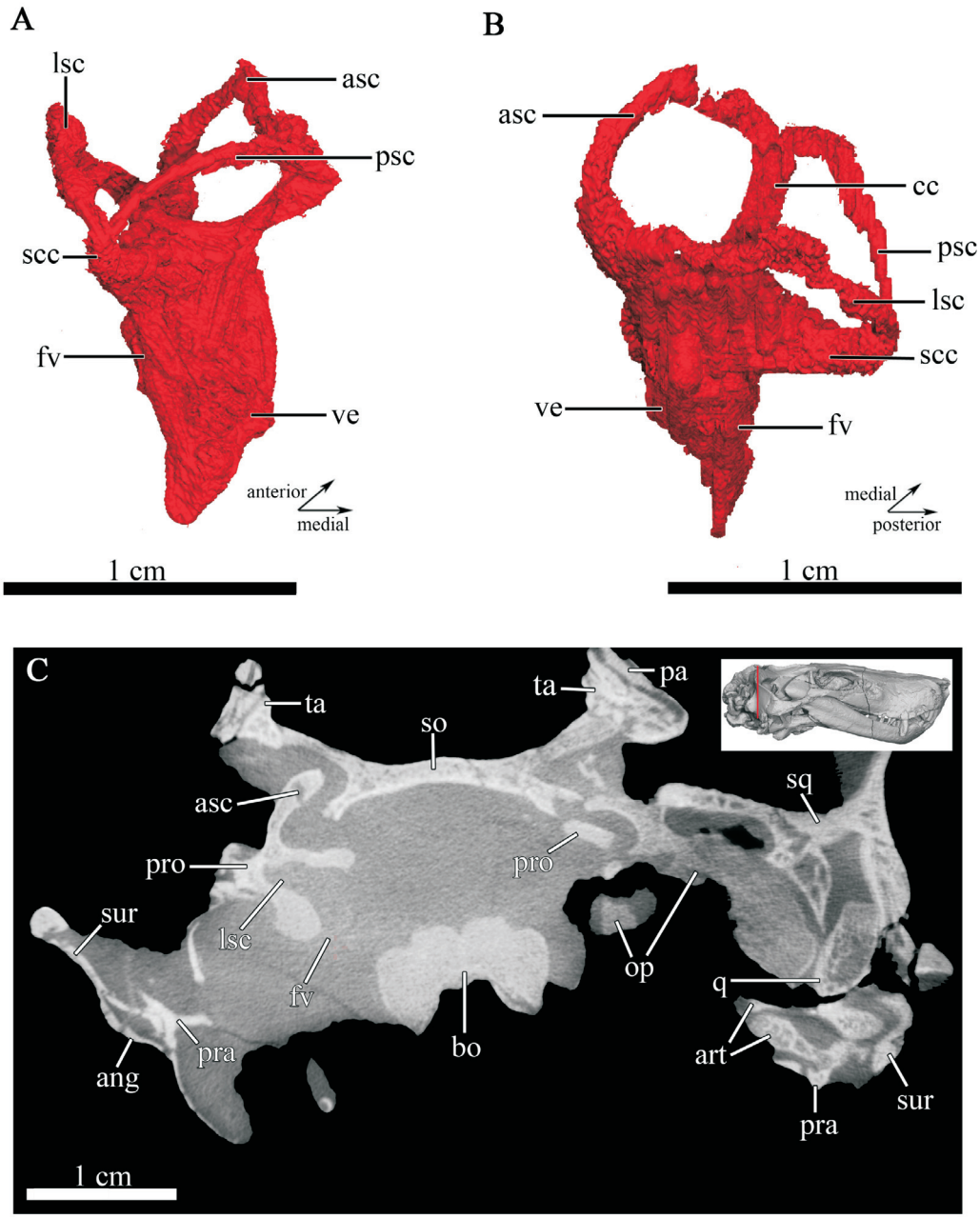


**Figure 16**. Three-dimensional reconstruction of the left bony labyrinth of BP/1/3849 in **A**, posterior and **B**, lateral view. **C**, Transverse CT section through the otic region of BP/1/3849. *Abbreviations*: ang, angular; art, articular; asc, anterior semicircular canal; bo, basioccipital; cc, crus communis; fv, fenestra vestibuli; lsc, lateral semicircular canal; op, opisthotic; pra, prearticular; pro, prootic; psc, posterior semicircular canal; q, quadrate; scc, secondary crus communis; sq, squamosal; so, supraoccipital; sur, surangular: ta, tabular; ve, vestibule.

Heever 1994) and are frequently missing even in well-preserved skulls.

*Inner ear*

Multiple bones of the basicranium contribute to the inner ear housing in BP/1/3849: the basioccipital, the supraoccipital, prootic, exoccipital, and opisthotic (Fig. 16C). Due to partial damage of the prootic and opisthotic bones, especially in the areas where they encircle the semicircular canals, it was not possible to visualize the courses of the semicircular canals for the right otic region adequately (Fig. 17). Hence, only the overall better preserved left otic region permitted reconstruction of most of the inner ear (Figs 16, 17) of BP/1/3849 with confidence. This side still shows some deformation, however. As the left prootic has been slightly shifted upwards, it was somewhat difficult to determine the exact course of the anterior semicircular canal in the CT data, which originates dorsally from the posterior apex of the crus communis and curves downwards to join the anterior ampullar recess. Though the supraoccipital is slightly deformed and has also been shifted inside the brain cavity, the position of the crus communis, whose dorsal limit is defined by the supraoccipital, and the course of the posterior semicircular canal, which is also partially defined by the supraoccipital, are clearly visible in the CT data. The posterior semicircular canal appears to have emerged roughly at the same level from the posterior apex of the crus communis as the anterior canal and curves downwards to join the posterior ampullar recess. The anterior semicircular canal is wider (at 6.06 mm) than the posterior canal (4.07 mm), but they are of nearly equiva-

lent height (anterior 4.74 mm and posterior 4.58 mm). The lateral (horizontal) semicircular canal is the widest of the three semicircular canals with a width of 7.93 mm, but is not as tall as the anterior and posterior canal, having a height of 3.45 mm. The anterior semicircular canal appears to be the longest of the three semicircular canals, as in most non-mammalian therapsids and mammals (e.g. Olson 1944; Luo 2001; Kielan-Jaworowska *et al*. 2004; Rodrigues *et al*. 2013; Benoit *et al*. 2021), with a possible length of 11.94 mm, based on our interpretation of where it might have curved around dorsally to join the crus communis, followed by the lateral (horizontal) semicircular canal, which is 10.70 mm long, and the posterior semicircular canal, which is 8.86 mm. Between the posterior and lateral (horizontal) semicircular canals, a secondary crus communis is developed, a feature known for all non-mammalian therapsids with reconstructed inner ears, except some biarmosuchians (e.g. Laaß 2014; Benoit *et al*. 2017b; Araújo *et al*. 2018; Bendel *et al*. 2018; Pusch *et al*. 2019, 2020).

The bony housing of the vestibule is formed by the prootic, opisthotic, basioccipital, and exoccipital, of which the prootic forms its anterior and the opisthotic its posterior border. Together, both bones also contribute to its lateral wall, whereas the basioccipital and the overlying exoccipital form its medial border. It is slightly curved and subtriangular in shape and is 8.41 mm long and 3.17 mm wide. As in various cynodonts, such as *Cynosaurus*, *Galesaurus*, *Thrinaxodon*, *Massetognathus*, and *Brasilodon* ('*Brasilitherium*') (Rodrigues *et al*. 2013; Benoit *et al*. 2017b: figs 4I,J,K; Pusch *et al*. 2019) and the anomodont *Niassodon* (Castanhinha *et al*. 2013), the fenestra vestibuli faces laterally (Figs 16, 17). This contrasts with what has been described for the baurioid *Microgomphodon* (Benoit *et al*. 2017b: fig. 4D), the basal therocephalian *Lycosuchus* (Pusch *et al*. 2020), and most other non-cynodont therapsids with described inner ears (e.g. Laaß 2014; Benoit *et al*. 2017b, 2021; Araújo *et al*. 2018; Bendel *et al*. 2018), in which the fenestra vestibuli is located at the ventrolateral end of the vestibule. However, unlike in cynodonts and a few non-cynodont therapsids, namely the biarmosuchian *Lemurosaurus*, the anomodonts *Niassodon* and *Pristerodon*, and the therocephalians *Lycosuchus* and *Microgomphodon* (Luo 2001; Kielan-Jaworowska *et al*. 2004; Castanhinha *et al*. 2013; Laaß 2015; Benoit *et al*. 2017b; Pusch *et al*. 2019, 2020), no cochlear recess is ventrally differentiated from the main part of the vestibule.

**Brain endocast**

The calculated volume of the reconstructed brain endocast of BP/1/3849 is 3470.26 $mm^3$. The total length adds up to 3.11 mm. This was measured from the anteriormost edge of the olfactory bulbs to the posterior margin of the foramen magnum. The maximum width of the brain endocast is given by the distance between the lateral limits of the paraflocculi and is 23.98 mm. The maximum height was measured from the dorsal edge of the forebrain where the cast of the pineal body is situated to the level of the ventral margin of the hypophysis and is approximately 17.79 mm (recognizing that this is the most uncertain of the measures due to limited ossified ventral boundaries of the brain). The general morphology of the brain endocast of BP/1/3849 resembles that described for other non-mammaliaform therapsids in having relatively narrow (compared to mammals) olfactory bulbs, a narrow, long and tubular forebrain (cerebrum) with undifferentiated cerebral hemispheres (due to the absence of a median sulcus/longitudinal fissure), and a hindbrain (cerebellum) that is shorter and wider than the forebrain region and thus displays the plesiomorphic condition (Fig. 17) (see e.g. Kielan-Jaworowska *et al*. 2004; Rowe *et al*. 2011; Laaß 2015; Araújo *et al*. 2017; Bendel *et al*. 2018; Pavanatto *et al*. 2019; Pusch *et al*. 2019; Huttenlocker & Sidor 2020).

The anteriormost part of the brain endocast is formed by the olfactory bulbs, which are slightly anteroposteriorly convex in lateral view and separated from each other by a slight median sulcus (Fig. 17B,D). The sphenethmoid, when intact, would have joined the frontals to define the ventral limits and partial side wall of the olfactory bulbs and partially the forebrain, but is displaced from its *in situ* position in BP/1/3849. Thus, it was difficult to reconstruct the exact ventral expansion of the olfactory bulb casts. By contrast, their anterior limit is relatively well defined by the two anteroposteriorly running ridges on the ventral surface of the frontals (Fig. 10), which partially separate them from the hindmost part of the nasal cavity. Similar ridges have also been described for some other non-mammalian therapsids such as the gorgonopsian *Cynariops* (Bendel *et al*. 2018) and the cynodonts *Procynosuchus* (Kemp 1979), *Chiniquodon* (Kemp 2009), *Galesaurus* (Pusch *et al*. 2019), and *Bolotridon* (Pusch *et al*. 2021). The olfactory bulb casts are approximately 12.51 mm long and 10.20 mm wide.

The cast of the elongated and slender forebrain (cerebrum) bears the small pineal body on its dorsal surface, which is girdled by the parietal foramen. Comparable to the ventral limits of the olfactory bulbs, the ventral expansion of the forebrain cannot be determined with certainty due to the lack of bony structures between the frontals and pterygoids. The dorsal surface of the forebrain cast corresponds to the concave ventral surfaces of the frontal and parietal, which indicates that the forebrain was in close contact with the skull roof (Figs 7, 17).

The epipterygoids contribute to the partial sidewall of the unossified space posterior to the orbital vacuity just anterior to the paired pilae antoticae and define the maximum width of the brain in that region. However, the left epipterygoid is somewhat dislocated in BP/1/3849 (Fig. 4), with the dorsal portion of its ascending process, which has been strongly shifted into the brain cavity, making it difficult to define the maximum width of the brain in that region. Posterior to the epipterygoids and anterior to the pilae antoticae, the ventral limit of the brain endocast is marked by the shallow sella turcica of the parabasisphenoid (Fig. 11A) accommodating the cast of the hypophysis (Fig. 17D), forming the ventral portion of the midbrain region. The boundary between the latter and the forebrain region appears confluent on the endocast,

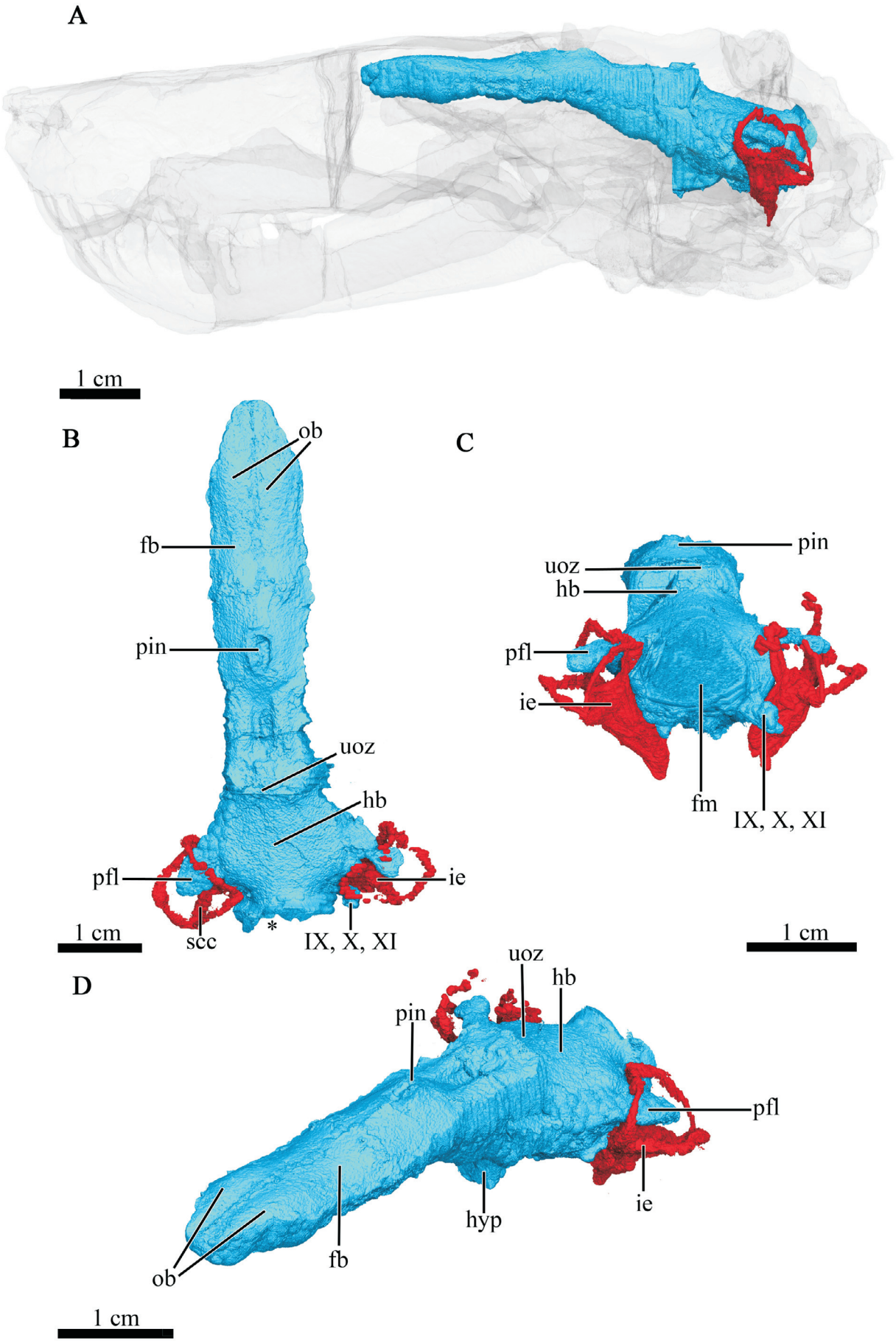


**Figure 17**. Three-dimensional reconstruction of the brain endocast (blue) with reconstructed inner ear labyrinth (red) of BP/1/3849 in **A**, left lateral view with the skull transparent, **B**, dorsal view, **C**, posterior view and **D**, anterodorsolateral view. Asterisk indicates the location of the foramen magnum. *Abbreviations*: fb, forebrain; fm, foramen magnum; hb, hindbrain; hyp, hypophysis; ie, inner ear; ob, olfactory bulbs; pfl, paraflocculus; pin, pineal body; scc, secondary crus communis; uoz 'unossified zone'; IX, X, XI, cast of the root of these cranial nerves.

with the dorsal portion of the midbrain showing a sharp bulge that fills an unossified space enclosed by the parietal, postparietal and supraoccipital. A comparable structure has also been described for cynodonts and the anomodonts *Pristerodon* and *Diictodon* (e.g. Olson 1944; Fourie 1974; Kemp 1979; Kielan-Jaworowska *et al*. 2004; Kemp 2009; Laaß 2015; Laaß *et al*. 2017; Pavanatto *et al*. 2018; Pusch *et al*. 2019; Huttenlocker & Sidor 2020). However, the exact shape of the bulge filling this unossified space is not well defined in BP/1/3849, due to compression of the dorsal occipital plate in that area (Fig. 11). Laaß *et al*. (2017) listed the following hypotheses as a possible explanation for what this zone could constitute: a possible middorsal vermis of the cerebellum (Kielan-Jaworowska *et al*. 2004; Rodrigues *et al*. 2014; Pusch *et al*. 2019), the unossified portion of the synotic tectum (Kemp 1979; Huttenlocker & Sidor 2020), the pineal gland (Kemp 2009), or a system of blood vessels associated with superior and transverse sinuses (Laaß *et al*. 2017; Pavanatto *et al*. 2019).The hindbrain (cerebellum) is situated posterior to the bulge of the unossified zone and the hypophyseal cast ventrally, where the endocast becomes wider. However, comparable to the confluent boundary between the fore- and midbrain, the exact border between the mid- and hindbrain regions also appears not well defined on the endocast. The roof of the confluent mid- and hindbrain cast appears to be exclusively formed by the supraoccipital, but it has been strongly shifted into the brain cavity due to compression of the dorsal occipital plate, preventing a contact of the brain endocast with the postparietal, which would have contributed to roofing the mid- and hindbrain region when intact. The dorsal surface of the brain endocast in that region is slightly convex, suggesting a close contact with the supraoccipital posterodorsally. In addition, its sloping dorsal surface appears strongly inclined as a result of the strong inclination of the supraoccipital. The floor of the mid- and hindbrain cavity is mainly shaped by the basioccipital, with contribution of the prootics and opisthotics ventrolaterally. The casts of the small paraflocculi are encircled by the anterior semicircular canal of the inner ear and protrude laterally on either side from the hindbrain (cerebellum). The parafloccculus is surrounded by the prootic, opisthotic, and supraoccipital, which encase the floccular fossa. The cast of the right parafloccculus is poorly visible on the endocasts however, because of damage to the prootic and opisthotic in the right otic region. The cast of the roots of cranial nerves IX, X, and IX are visible posteroventrally to the parafloccculus, which passed through the jugular foramen (Fig. 17B).

**Postcranial bones**

Although much of the anterior skeleton is preserved in BP/1/3849 (Brink 1965), description of the postcranial skeleton in this study is limited to the two cervical bones which are part of the atlas-axis complex, as only they were CT-scanned with the skull. One of them is just a fragment of a bone, probably part of the atlas pleurocentrum. It is represented by a roughly oval chunk of bone with a crescentic dorsomedial extension (Fig. 12B). Here we interpret this element as the left anterolateral margin of the atlas pleurocentrum. Alternatively, it could represent the proatlas, which would fit in terms of size and shape.

Dorsolateral to this fragment lies a larger cervical element, which we identify as the left atlantal neural arch. In dorsal view, it has a plate-like lateral expansion from which the medial margin appears tongue-like and overlies the anterolateral part of the atlas pleurocentrum. This region seems to be associated ventrally with the dorsomedial extension of the pleurocentrum.

## DISCUSSION

For the most part, *Olivierosuchus* exhibits a generalized craniomandibular morphology for an akidnognathid therocephalian. Although clearly diagnosable as a distinct taxon based on a combination of tooth count, palatine and pterygoid morphology, it shows many shared features with *Promoschorhynchus* and also overlaps in most cranial characters with basal akidnognathids such as *Annatherapsidus*, *Jiufengia*, and *Shiguaignathus*, while lacking the extreme morphologies seen in the brevirostrine taxa *Euchambersia* and *Moschorhinus*.

**Brain endocast shape and size in *Olivierosuchus* compared to that of other therapsids**

Neuroanatomically, *Olivierosuchus* exhibits many primitive features typical of non-mammalian therapsids, such as relatively narrow olfactory bulbs and small paraflocculi as well as an elongate, slender forebrain with undivided cerebral hemispheres.

It appears to have a relatively low synapsid encephalization quotient (EQS) value, below 1 (EQS = 0.87) (Table 2). Comparing this value with other therapsids (see Table 2), *Olivierosuchus* has a notably lower EQS than the other two Triassic therocephalians included in the dataset of Benoit *et al*. (2023), i.e. *Microgomphodon* and *Tetracynodon darti*, which are both above 1. As *Olivierosuchus* and *Tetracynodon darti* both lived immediately after the Permian-Triassic mass extinction, the contrast between their EQS suggests that brain size may not have been a decisive factor for surviving the crisis. Recent analyses by Dembitzer *et al*. (2022) indicated that relatively larger brain sizes in mammals were helpful to survive the Late Quaternary extinction. They hypothesized that larger brains enabled an enhanced behavioral plasticity and the ability to cope with the rapidly changing environment in the Late Quaternary, which was characterized by the rise of anthropogenic threats and climate change. By contrast, no consistent EQS trends are visible between late Permian and Early Triassic synapsids (Table 2), even among closely related taxa. The Early Triassic cynodonts *Platycraniellus* and *Galesaurus* are reconstructed as having EQS values well above 1.5, which is close to that calculated for some mammaliaforms, whereas the coeval *Thrinaxodon* has an EQS of approximately 1 and *Nythosaurus* has an EQS value below 1 (EQS = 0.78). Another Early Triassic survivor, the dicynodont *Lystrosaurus*, also has an EQS well below 1 (Table 2). This diversity of brain sizes among Early Triassic taxa suggests that behavioral plasticity as reflected by large brain size was not of utmost importance for

**Table 2**. Dataset of Body Mass (BM) and Endocranial Volume (EV) used to calculate the synapsid specific Encephalization Quotient ($EQ_{synapsid}$) modified from Benoit *et al*. (2023).

| Higher rank taxon | Genus | BM | EV | EQ synapsid |
|---|---|---|---|---|
| Therapsida | *Lemurosaurus* | 5219.17 | **4.02** | 0.86 |
| Therapsida | *Lemurosaurus* | 1327.12 | **1.75** | 0.94 |
| Therapsida | *Moschops* | 128 654.74 | **50.24** | 1.27 |
| Therapsida | *Struthiocephalus* | 288 175.73 | **65.00** | 0.95 |
| Therapsida | *Pristerodon* | 1480.74 | **2.18** | 1.09 |
| Therapsida | *Lystrosaurus* | 18 511.07 | **8.00** | 0.74 |
| Therapsida | *Kawingasaurus* | 211.94 | **1.09** | 2.00 |
| Therapsida | *Niassodon* | 782.06 | **1.06** | 0.81 |
| Therapsida | *Rastodon* | 1984.00 | **1.76** | 0.72 |
| Therapsida | Gorgonopsia indet. | 3043.00 | **4.62** | 1.42 |
| Therapsida | *Aelurosaurus* | 7255.45 | **6.00** | 1.03 |
| Therapsida | *Cyonosaurus* | 8636.64 | **6.77** | 1.04 |
| Therapsida | *Tetracynodon* | 1316.58 | **2.28** | 1.23 |
| Therapsida | *Microgomphodon* | 1797.04 | **2.36** | 1.03 |
| Therapsida | *Olivierosuchus* | 4165.00 | **3.47** | 0.87 |
| Basal cynodont | *Nythosaurus** | 1916.00 | **1.86** | 0.78 |
| Basal cynodont | *Galesaurus* | 669.00 | **2.75** | 2.33 |
| Basal cynodont | *Galesaurus* | 1984.00 | **2.48** | 1.02 |
| Basal cynodont | *Platycraniellus* | 2863.00 | **5.56** | 1.78 |
| Basal cynodont | *Thrinaxodon* | 1010.05 | **1.56** | 1.00 |
| Basal cynodont | *Thrinaxodon* | 700.00 | **1.46** | 1.20 |
| Cynognathia | *Diademodon* | 77 402.98 | **26.97** | 0.95 |
| Cynognathia | *Diademodon* | 7000.00 | **8.00** | 1.41 |
| Cynognathia | *Trirachodon* | 3124.71 | **2.15** | 0.65 |
| Cynognathia | *Langbergia* | 2614.00 | **2.3** | 0.78 |
| Cynognathia | *Andescynodon* | 1071.04 | **1.11** | 0.69 |
| Cynognathia | *Andescynodon* | 1397.04 | **1.10** | 0.57 |
| Cynognathia | *Massetognathus* | 2677.43 | **3.163** | 1.06 |
| Cynognathia | *Massetognathus* | 1316.58 | **1.56** | 0.84 |
| Cynognathia | *Massetognathus* | 6128.85 | **2.86** | 0.55 |
| Cynognathia | *Massetognathus* | 2237.67 | **2.81** | 1.06 |
| Cynognathia | *Siriusgnathus* | 34 262.15 | **28.80** | 1.76 |
| Cynognathia | *Exaeretodon* | 69 496.56 | **15.98** | 0.61 |
| Cynognathia | *Exaeretodon* | 36 435.56 | **26.43** | 1.55 |
| Cynognathia | *Exaeretodon* | 15 061.15 | **11.47** | 1.21 |
| Probainognathia | *Probelesodon* | 5417.25 | **4.02** | 0.84 |
| Probainognathia | *Probelesodon* | 4763.56 | **2.60** | 0.59 |
| Probainognathia | *Probainognathus* | 858.43 | **1.12** | 0.81 |
| Probainognathia | *Therioherpeton* | 97.85 | **0.29** | 0.90 |
| Probainognathia | *Riograndia* | 71.15 | **0.32** | 1.22 |
| Probainognathia | *Tritylodon* | 5617.00 | **5.27** | 1.08 |
| Probainognathia | *Tritylodon* | 6278.35 | **5.06** | 0.96 |
| Probainognathia | *Tritylodon* | 6278.35 | **5.06** | 0.96 |
| Probainognathia | *Tritylodon* | 8759.68 | **6.30** | 0.96 |
| Probainognathia | *Brasilodon* | 98.67 | **0.24** | 0.74 |
| Early Mammaliaformes | *Morganucodon* | 51.00 | **0.33** | 1.54 |
| Early Mammaliaformes | *Hadrocodium* | 2.75 | **0.04** | 1.31 |
| Mammalia | *Vintana* | 8950.00 | **15.64** | 2.34 |
| Mammalia | *Triconodon* | 138.00 | **0.82** | 2.00 |
| Mammalia | *Litovoi* | 166.00 | **0.73** | 1.57 |
| Mammalia | *Chulsanbaatar* | 13.30 | **0.22** | 2.57 |
| Mammalia | *Kryptobaatar* | 28.18 | **0.32** | 2.28 |
| Mammalia | *Vincelestes* | 619.00 | **2.12** | 1.89 |
| Mammalia | *Kennalestes* | 39.00 | **0.30** | 1.70 |
| Mammalia | *Asioryctes* | 43.20 | **0.50** | 2.65 |
| Mammalia | *Zalambdalestes* | 82.69 | **1.02** | 3.50 |

*Pusch *et al*. (2023).

therapsids of that time, perhaps because unlike large mammals in the Late Quaternary they were not competing against other large-brained, relatively intelligent species. These data may also reflect the high degree of uncertainty in endocast reconstruction (due to incomplete ossification of the braincase) and body mass estimates (as few taxa are known from complete skeletons, and existing proxies based on mammals and dinosaurs appear problematic for earlier-diverging amniotes; see e.g. Romano & Manucci 2019) for early synapsids, making determination of their EQS values a much more fraught endeavour than for Quaternary mammals.

### Variation in bony labyrinth morphology in therapsids

Similar to the brain endocast, the overall morphology of the inner ear endocast in BP/1/3849 is in keeping with usual patterns in non-mammalian therapsids. The shape of the vestibule is rather broad and subtriangular in lateral view, like that of most early therapsids (with a few exceptions, such as *Euchambersia* and the dicynodont *Kawingasaurus*; Laaß 2014; Benoit *et al*. 2017b). The fenestra vestibuli in BP/1/3849 faces laterally from the vestibule, as in various cynodonts like *Cynosaurus*, *Galesaurus*, *Thrinaxodon*, *Massetognathus*, and *Brasilodon* (Rodrigues *et al*. 2013; Benoit *et al*. 2017b: figs 4I,J,K; Pusch *et al*. 2019) and the anomodont *Niassodon* (Castanhinha *et al*. 2013), but differs from the condition in most other non-cynodont therapsids, including therocephalians such as *Microgomphodon* (e.g. Laaß 2016; Benoit *et al*. 2017b,d, 2021; Araújo *et al*. 2018; Bendel *et al*. 2018).

The cochlear recess is absent in BP/1/3849. This is the condition observed in most of its therocephalian relatives for which the otic region has been visualized, except for *Microgomphodon* and *Lycosuchus*, in which the recess is present (Benoit *et al*. 2017b; Pusch *et al*. 2020), and differs from the typical cynodont condition, where a cochlear recess is usually present. Outside of Cynodontia, the cochlear recess is only known for two anomodonts (*Niassodon mfumukasi* and *Pristerodon mackayi*), one biarmosuchian (*Lemurosaurus pricei*) and the two aforementioned therocephalians (Castanhinha *et al*. 2013; Laaß 2015; Benoit *et al*. 2017b). Pusch *et al*. (2020) emphasized that limited sampling in Therocephalia made it uncertain whether absence of this recess is really typical of the clade (the condition in *Lycosuchus* suggests it was ancestrally present), and the same can be said for all other non-cynodont therapsid clades. Benoit *et al*. (2017b) proposed that a distinct cochlear recess likely evolved multiple times among therapsids.

## CONCLUSIONS

Although it has been the centre of a few previous descriptions (Brink 1965; Botha-Brink & Modesto 2011), many aspects of the anatomy, and particularly the endocranial anatomy, of *Olivierosuchus parringtoni* have historically been poorly known. Our use of computed tomography and 3D-modelling have provided novel insights into the cranial anatomy of *Olivierosuchus* and have permitted a broader understanding of its morphology in the context of other akidnognathids and non-mammalian therapsids generally. These new data support the idea of neurological conservatism in therapsids outside of advanced cynodonts. There are a few characters that appear to show variability within Therocephalia,

however, such as the orientation of the fenestra vestibuli and the presence/absence of the cochlear recess, which are worth further scrutiny as endocast sampling in the clade increases.

Moreover, a comparative analysis of cranial features highlighted areas of variability within the akidnognathid clade. *Olivierosuchus parringtoni* shows many conserved features of external cranial morphology present in basal akidnognathids and different from the highly specialized *Euchambersia* and *Moschorhinus*. Although suggestive of a close relationship between the latter two taxa, redescription and taxonomic revision of the array of other small akidnognathids from the Karoo Basin is necessary, especially poorly known taxa such as *Cerdosuchoides* that have been recovered as the closest relatives of *Moschorhinus* in recent phylogenies (e.g. Liu & Abdala 2022). The role of akidnognathids in the Early Triassic recovery following the most severe mass extinction event in Earth's history also requires additional attention. *Olivierosuchus* appears to be a reasonably abundant and stratigraphically long-ranging taxon (at least among those taxa restricted to the *Lystrosaurus declivis* AZ), yet akidnognathids as a whole seem to be a 'dead clade walking' in the Triassic, having survived the extinction but not diversifying in its wake, and dying out before the end of the Early Triassic. Understanding why *Olivierosuchus* proved an evolutionary dead end while baurioid therocephalians and cynodonts underwent major radiations at this time requires more detailed information on the palaeobiology and distribution of these taxa than is currently available. More anatomical data relevant to neurobiology and functional morphology of Early Triassic therapsids, such as those provided here for *Olivierosuchus*, are needed, with baurioids being particularly undersampled at present and a prime target for CT-assisted study.

We wish to thank Kuda Jakata for aid in scanning BP/1/3849, and the Deutsche Forschungsgemeinschaft (DFG) grant number FR 2457/8-1, the Palaeontological Scientific Trust (PAST), GENUS – DST-NRF Centre of Excellence in Palaeosciences, and the DST-NRF African Origins program for financial support of this study. For access to comparative materials, C.F.K. thanks Nonhlanhla Mchunu (CGS), Sifelani Jirah and Bernhard Zipfel (ESI), Paul Barrett and the late Angela Milner (NHMUK), Jennifer Botha and Elize Butler (formerly of NMQR), and Claire Browning and Zaituna Skosan (SAM). In the framework of this Festschrift in honor of Bruce Rubidge, the authors and particularly the senior author J.F. would like to express their sincerest and warmest gratitude to Bruce for his continued and inspiring exchange of ideas and hospitality at various occasions. Finally, we are grateful to the reviewers Brandon Stuart and Trond Sigurdsen and the editor Kimberley Chapelle for their improvements to the manuscript.

## DATA AVAILABILITY STATEMENT

For requests concerning access to CT scan data on BP/1/3849, please contact Julien Benoit (julien.benoit@wits.ac.za), Bernhard Zipfel (Collection manager, ESI: bernhard.zipfel@wits.ac.za), and Gideon Chinamatira (CT facility manager, ESI: 2340386@students.wits.ac.za).

## ABBREVIATIONS

**Institutional**

| | |
|---|---|
| BP | Evolutionary Studies Institute, University of the Witwatersrand, Johannesburg, South Africa |
| CGS | Council for Geosciences, Pretoria, South Africa |
| IVPP | Institute of Vertebrate Paleontology and Paleoanthropology, Chinese Academy of Sciences, Beijing, China |
| NHMUK | Natural History Museum, London, United Kingdom |
| NMQR | National Museum, Bloemfontein, South Africa |
| PMO | former Paleontological Museum of Oslo, now incorporated in the Natural History Museum, University of Oslo, Norway |
| SAM | Iziko South African Museum, Cape Town, South Africa |

**§ORCID iDs**

A. Gigliotti : orcid.org/0009-0001-9443-6184
L.C. Pusch: orcid.org/0000-0003-1219-6824
C.F. Kammerer: orcid.org/0000-0002-0596-623X
J. Benoit: orcid.org/0000-0001-5378-3940
J. Fröbisch: orcid.org/0000-0002-2501-9387

## REFERENCES

ABDALA, F., RUBIDGE, B.S. & VAN DEN HEEVER, J. 2008. The oldest therocephalians (Therapsida, Eutheriodontia) and the early diversification of Therapsida. *Palaeontology* **51**, 1011–1024.

ABDALA, F., JASHASHVILI, T., RUBIDGE, B.S. & VAN DEN HEEVER, J. 2014. New material of *Microgomphodon oligocynus* (Eutherapsida, Therocephalia) and the taxonomy of southern African Bauriidae. **In**: Kammerer C.F. & Angielczyk & K.D. Fröbisch, J. (eds), *Early Evolutionary History of the Synapsida*, 209–231. Dordrecht, Springer.

ANGIELCZYK, K.D. & KAMMERER, C.F. 2018. Non-mammalian synapsids: the deep roots of the mammalian family tree. **In**: Zachos, F.E. & Asher, R.J. (eds), *Handbook of Zoology. Mammalian Evolution, Diversity and Systematics*, 117–199. Berlin, DeGruyter.

ARAÚJO, R., FERNANDEZ, V., POLCYN, M.J., FRÖBISCH, J. & MARTINS, R.M.S. 2017. Aspects of gorgonopsian paleobiology and evolution: insights from the basicranium, occiput, osseous labyrinth, vasculature, and neuroanatomy. *PeerJ* **5**, e3119.
DOI: 10.7717/peerj.3119

ARAÚJO, R., FERNANDEZ, V., RABBITT, R.D., EKDALE, E.G., ANTUNES, M.T., CASTANHINHA, R., FRÖBISCH, J. & MARTINS, R.M.S. 2018. *Endothiodon* cf. *bathystoma* (Synapsida: Dicynodontia) bony labyrinth anatomy, variation and body mass estimates. *PLOS ONE* **13**(3), e0189883.
DOI: 10.1371/journal.pone.0189883

BARRY, T.H. 1965. On the epipterygoid-alisphenoid transition in Therapsida. *Annals of the South African Museum* **48**, 399–426.

BENDEL, E-M., KAMMERER, C.F., KARDJILOV, N., FERNANDEZ, V. & FRÖBISCH, J. 2018. Cranial anatomy of the gorgonopsian *Cynariops robustus* based on CT-reconstruction. *PLOS ONE*, **13**(11), e0207367.
https://doi.org/10.1371/journal.pone.0207367

BENOIT, J., MANGER, P. & RUBIDGE, B.S. 2016a. Palaeoneurological clues to the evolution of defining mammalian soft tissue traits. *Scientific Reports* **6**, 25604.
https://doi.org/10.1038/srep25604

BENOIT, J., DOLLMAN, K.N., SMITH, R.M.H. & MANGER, P.R. 2023. At the root of the mammalian mind: the sensory organs, brain and behavior of pre-mammalian synapsids. **In**: Calvey, T., de Sousa, A.A. & Beaudet, A, (eds), *Progress in Brain Research* **275**, 25–72. Elsevier.

BENOIT, J., FERNANDEZ, V., MANGER, P.R. & RUBIDGE, B.S. 2017d. Endocranial casts of pre-mammalian therapsids reveal an unexpected neurological diversity at the deep evolutionary root of mammals. *Brain, Behavior and Evolution* **90**(4), 311–333.

BENOIT, J., JASINOSKI, S.C., FERNANDEZ, V. & ABDALA, F. 2017a: The mystery of a missing bone: revealing the orbitosphenoid in basal Epicynodontia (Cynodontia, Therapsida) through computed tomography. *The Science of Nature* **104**(66), 1–10.
https://doi.org/10.1007/s00114-017-1487-z

BENOIT, J., MANGER, P.R., FERNANDEZ, V. & RUBIDGE, B.S. 2016b. Cranial bosses of of *Choerosaurus dejageri* (Therapsida, Therocephalia): earliest evidence of cranial display structures in eutheriodonts. *PLOS ONE* **11**, e0161457.
https://doi.org/10.1371/journal.pone.0161457

BENOIT, J., MANGER, P.R., FERNANDEZ, V. & RUBIDGE, B.S. 2017b. The bony labyrinth of late Permian Biarmosuchia: palaeobiology and diversity in non-mammalian Therapsida. *Palaeontologia africana* **52**, 58–77.

BENOIT, J., NORTON, L.A., MANGER, P.R. & RUBIDGE B.S. 2017c. Reappraisal of the envenoming capacity of *Euchambersia mirabilis* (Therapsida, Therocephalia) using $\mu$CT-scanning techniques. *PLOS ONE* **12**(2), e0172047.
https:/doi.org/10.1371/journal pone.0172047

BENOIT, J., KRUGER, A., JIRAH, S., FERNANDEZ, V. & RUBIDGE, B.S. 2021. Palaeoneurology and palaeobiology of the dinocephalian therapsid *Anteosaurus magnificus*. *Acta Palaeontologica Polonica* **66**(1), 29–39.
https://doi.org/10.4202/app.00800.2020

BENOIT, J., ANGIELCZYK, K.D., MIYAMAE, J.A., MANGER, P.,

FERNANDEZ, V. & RUBIDGE, B. 2018. Evolution of facial innervation in anomodont therapsids (Synapsida): insights from X-ray computerized microtomography. *Journal of Morphology* **279**, 673–701. https://doi.org/10.1002/jmor.20804
BENOIT, J., RUF, I., MIYAMAE, J.A., FERNANDEZ, V., RODRIGUES, P.G. & RUBIDGE, B.S. 2019. The evolution of the maxillary canal in Probainognathia (Cynodontia, Synapsida): reassessment of the homology of the infraorbital foramen in mammalian ancestors. *Journal of Mammalian Evolution* **27**, 329–348. https://doi.org/10.1007/s10914-019-09467-8
BOONSTRA, L.D. 1972. Discard the names Theriodontia and Anomodontia: a new classification of the Therapsida. *Annals of the South African Museum* **59**, 315–338.
BOTHA, J. & SMITH, R.M.H. 2020. Biostratigraphy of the *Lystrosaurus declivis* Assemblage Zone (Beaufort Group, Karoo Supergroup), South Africa. *South African Journal of Geology*, 123(2), 207–216. https://doi.org/10.25131/sajg.123.0015
BOTHA-BRINK, J. & MODESTO, S.P. 2011. A new skeleton of the therocephalian synapsid *Olivierosuchus parringtoni* from the Lower Triassic South African Karoo Basin. *Palaeontology* **54**(3), 591–606.
BOTHA-BRINK, J., HUTTENLOCKER, A.K. & MODESTO, S.P. 2014. Vertebrate paleontology of Nooitgedacht 68: a *Lystrosaurus maccaigi*-rich Permo-Triassic boundary locality in South Africa. **In**: Kammerer, C.F., Angielczyk, K.D. & Fröbisch, J. (eds), *Early Evolutionary History of the Synapsida*, 289–304. Dordrecht, Springer.
BRINK, A.S. 1963. The taxonomic position of Synapsida. *South African Journal of Science* **59**, 153–159.
BRINK, A.S. 1965. A new ictidosuchid (Scaloposauria) from the Lystrosaurus-Zone. *Palaeontologia africana* 9, 129–139.
BRINK, A.S. 1986. Illustrated bibliographic catalogue of the Synapsida. *Department of Mineral and Energy Affairs Handbook* **10**.
BROCKLEHURST, N. 2019. Morphological evolution in therocephalians breaks the hypercarnivore ratchet. *Proceedings of the Royal Society B* **286**, 20190590.
CASTANHINHA, R., ARAÚJO, R., JÚNIOR, L.C., ANGIELCZYK, K.D., MARTINS, G.G., MARTINS, R.M.S., CHAOUIYA, C., BECKMANN, F. & WILDE, F. 2013. Bringing dicynodonts back to life: paleobiology and anatomy of a new emydopoid genus from the Upper Permian of Mozambique. *PLOS ONE* **8**(12), e80974. DOI: 10.1371/journal.pone.0080974
COLBERT, E.H. & KITCHING, J.W. 1981. Scaloposaurian reptiles from the Triassic of Antarctica. *American Museum Novitates* **2709**, 1–22.
CROMPTON, A.W. 2013. Evolution of the mammalian nose, presentation. Available at https://crompton.oeb.harvard.edu/evolution-mammalian-nose-presentation (accessed April 2022).
CROMPTON, A.W., MUSINSKY, C. & OWERKOWICZ, T. 2015. Evolution of the mammalian nose. **In**: Dial, K.P., Shubin, N. & Brainerd, E. (eds), *Great Transformations in Vertebrate Evolution*, 189–203. Chicago, University of Chicago Press.
CROMPTON, A.W., OWERKOWICZ, T. & MUSINSKY, C. 2017. Structure of the nasal region of non-mammalian cynodonts and mammaliaforms: speculations on the evolution of mammalian endothermy. *Journal of Vertebrate Paleontology* **37**, e1269116-3.
DEMBITZER, J., CASTIGLIONE, S., RAIA, P. & MEIRI, S. 2022. Small brains predisposed Late Quaternary mammals to extinction. *Scientific Reports* **12,** 3453. https://doi.org/10.1038/s41598-022-07327-9
DURAND, J.F. 1991. A revised description of the skull of *Moschorhinus* (Therapsida, Therocephalia). *Annals of the South African Museum* **99**, 381–413.
FOURIE, H. & RUBIDGE, B.S. 2007. The postcranial skeletal anatomy of the therocephalian *Regisaurus* (Therapsida: Regisauridae) and its utilization for biostratigraphic correlation. *Palaeontologia africana* **42**, 1–16.
FOURIE, S. 1974. The cranial morphology of *Thrinaxodon liorhinus*. *Annals of the South African Museum* **65**, 337–400.
FINDLAY, G.H. 1968. On the scaloposaurid skull of *Olivieria parringtoni* Brink with a note on the origin of hair. *Palaeontologia africana* **11**, 47–61.
GRUNERT, H.R., BROCKLEHURST, N. & FRÖBISCH, J. 2019. Diversity and disparity of Therocephalia: macroevolutionary patterns through two mass extinctions. *Scientific Reports* **9**(1), 5063.
HILLENIUS, W.J. 1991. The evolution of nasal turbinates and mammalian endothermy. *Paleobiology* **18**, 17–29.
HILLENIUS, W.J. 1994. Turbinates in therapsids: evidence for Late Permian origins of mammalian endothermy. *Evolution* **48**, 207–229.
HILLENIUS, W. J. & RUBEN, J.A. 2004. The evolution of endothermy in terrestrial vertebrates: who? when? why? *Physiological and Biochemical Zoology: Ecological and Evolutionary Approaches* **77**, 1019–1042.
HOPSON, J.A. & BARGHUSEN, H. 1986. An analysis of therapsid relationships. **In**: Hotton, N., MacLean, P.D., Roth, J.J. & Roth, E.C. (eds), *The Ecology and Biology of Mammal-like Reptiles*, 83–106. Washington, Smithsonian Institution Press.
HUTTENLOCKER, A. 2009. An investigation into the cladistic relationships and monophyly of therocephalian therapsids (Amniota: Synapsida). *Zoological Journal of the Linnean Society* **157**, 865–891. https://doi.org/10.1111/j.1096-3642.2009.00538.x
HUTTENLOCKER, A.K. & ABDALA, F. 2015. Revision of the first therocephalian, *Theriognathus* Owen (Therapsida: Whaitsiidae), and implications for cranial ontogeny and allometry in nonmammaliaform eutheriodonts. *Journal of Paleontology* **89**(4), 645–64. https://doi.org/10.1017/jpa.2015.32
HUTTENLOCKER, A.K. & BOTHA-BRINK, J. 2014. Bone microstructure and the evolution of growth patterns in Permo-Triassic therocephalians (Amniota, Therapsida). *PeerJ* **2**:e325.
HUTTENLOCKER, A.K. & SIDOR, C.A. 2016. The first karenitid (Therapsida, Therocephalia) from the upper Permian of Gondwana and the biogeography of Permo-Triassic therocephalians. *Journal of Vertebrate Paleontology* **36**, e1111897.
HUTTENLOCKER, A.K. & SIDOR, C.A. 2020. A basal non-mammaliaform cynodont from the Permian of Zambia and the origins of mammalian endocranial and postcranial anatomy. *Journal of Vertebrate Paleontology* **40**(5), e1827413. https://doi.org/10.1080/02724634.2020.1827413
HUTTENLOCKER, A.K. & SMITH, R.M.H. 2017. New whaitsioids (Therapsida: Therocephalia) from the Teekloof Formation of South Africa and therocephalian diversity during the end-Guadalupian extinction. *PeerJ* **5**:e3868.
HUTTENLOCKER, A.K., SIDOR, C.A. & ANGIELCZYK, K.D. 2015. A new eutherocephalian (Therapsida: Therocephalia) from the upper Madumabisa Mudstone Formation (Luangwa Basin) of Zambia. *Journal of Vertebrate Paleontology* **35**, e969400.
HUTTENLOCKER, A.K., SIDOR, C.A. & SMITH, R.M.H. 2011. A new specimen of *Promoschorhynchus* (Therapsida: Therocephalia: Akidnognathidae) from the Lower Triassic of South Africa and its implications for theriodont survivorship across the Permo-Triassic boundary. *Journal of Vertebrate Paleontology* **31**, 405–421.
KAMMERER, C.F. 2023. Revision of the Scylacosauridae (Therapsida: Therocephalia). *Palaeontologia africana* **56**, 51–87.
KAMMERER, C.F. & MASYUTIN, V. 2018. A new therocephalian (*Gorynychus masyutinae* gen. et sp. nov.) from the Permian Kotelnich locality, Kirov Region, Russia. *PeerJ* **6**, e4933.
KAMMERER, C.F. & SIDOR, C.A. 2002. Replacement names for the therapsid genera *Criocephalus* Broom 1928 and *Olivieria* Brink 1965. *Palaeontologia africana* **38**, 71–72.
KAMMERER, C.F., VIGLIETTI, P.A., BUTLER, E. & BOTHA, J. 2023. Rapid turnover of top predators in African terrestrial faunas around the Permian-Triassic mass extinction. *Current Biology* **33**, 2283–2290.
KEMP, T.S. 1979. The primitive cynodont *Procynosuchus*: functional anatomy of the skull and relationships. *Philosophical Transactions of the Royal Society of London B* **285**, 73–122.
KEMP, T.S. 2005. *The Origin and Evolution of Mammals*. Oxford, Oxford University Press.
KEMP, T.S. 2009. The endocranial cavity of a nonmammalian eucynodont, *Chiniquodon theotenicus*, and its implications for the origin of the mammalian brain. *Journal of Vertebrate Paleontology* **29**, 1188–1198.
KIELAN-JAWOROWSKA. Z., CIFELLI, R.L. & LUO, Z-X. 2004. *Mammals from the Age of Dinosaurs: Origin, Evolution, and Structure*. New York, Columbia University Press, 630 pp.
LAAß, M. 2014. Bone-conduction hearing and seismic sensitivity of the late Permian anomodont *Kawingasaurus fossilis*. *Journal of Morphology* **276**, 121–143.
LAAß, M. 2015. Virtual reconstruction and description of the cranial endocast of *Pristerodon mackayi* (Therapsida, Anomodontia). *Journal of Morphology* **276**, 1089–1099.
LAAß, M., SCHILLINGER, B. & KAESTNER, A. 2017. What did the "unossified zone" of the non-mammalian therapsid braincase house? *Journal of Morphology* **278**, 1020–1032. https://doi.org/10.1002/jmor.20583
LIU, J. & ABDALA, F. 2017. The tetrapod fauna of the upper Permian Naobaoguo Formation of China: 1. *Shiguaignathus wangi* gen et sp. nov., the first akidnognathid therocephalian from China. *PeerJ*, **5**, e4150.
LIU, J. & ABDALA, F. 2019. The tetrapod fauna of the upper Permian Naobaogou Formation of China: 3. *Jiufengia jiai* gen. et sp. nov., a large akidnognathid therocephalian. *PeerJ* **7**, e6463.
LIU, J. & ABDALA, F. 2022. The emblematic South African therocephalian *Euchambersia* in China: a new link in the dispersal of late Permian vertebrates across Pangea. *Biology Letters* **18**, 20220222.

LIU, J. & ABDALA, F. 2023. Late Permian terrestrial faunal connections invigorated: the first whaitsioid therocephalian from China. *Palaeontologia africana* **56**, 111–117.
LUO, Z-X. 2001. The inner ear and its bony housing in tritylodontids and implications for evolution of the mammalian ear. *Bulletin of the Museum of Comparative Zoology* **156**, 81–97.
LUO, Z-X. & CROMPTON, A.W. 1994. Transformation of the quadrate (incus) through the transition from non-mammalian cynodonts to mammals. *Journal of Vertebrate Paleontology* **14**, 341–374.
LUO, Z-X., KIELAN-JAWOROWSKA, Z. & CIFELLI, R.L. 2004. Evolution of dental replacement in mammals. *Bulletin of Carnegie Museum of Natural History* **2004**, 159–174.
MENDREZ, P.H. 1974. A new specimen of *Promoschorhynchus platyrhinus* Brink 1954 (Moschorhinidae) from the Daptocephalus-Zone (Upper Permian) of South Africa. *Palaeontologia africana* **17**, 69–85.
OLROYD, S.L. & SIDOR, C.A. 2022. Nomenclature, comparative anatomy, and evolution of the reflected lamina of the angular in non-mammalian synapsids. *Journal of Vertebrate Paleontology* **42**, e2101923.
https://doi.org/10.1080/02724634.2022.2101923
OLSON, E.C. 1944. Origin of mammals based upon cranial morphology of the therapsid suborders. *Geological Society of American Special Papers* **55**, 1–130.
PAVANATTO, A.E.B., KERBER L. & DIAS-DA-SILVA, S. 2019. Virtual reconstruction of cranial endocasts of traversodontid cynodonts (Eucynodontia: Gomphodontia) from the upper Triassic of southern Brazil. *Journal of Morphology* **280**, 1267–1281.
DOI: 10.1002/jmor.21029
PUSCH, L.C., KAMMERER, C.F. & FRÖBISCH, J. 2019. Cranial anatomy of the early cynodont *Galesaurus planiceps* and the origin of mammalian endocranial characters. *Journal of Anatomy* **234**(5), 592–621.
https://doi.org/10.1111/joa.12958
PUSCH, L.C., KAMMERER, C.F. & FRÖBISCH, J. 2021. Cranial anatomy of *Bolotridon frerensis*, an enigmatic cynodont from the Middle Triassic of South Africa, and its phylogenetic significance. *PeerJ* **9**, e11542.
https://doi.org/10.7717/peerj.11542
PUSCH, L.C., KAMMERER, C.F., FERNANDEZ, V. & FRÖBISCH, J. 2023. Cranial anatomy of the early cynodont *Nythosaurus larvatus* Owen, 1876, an Early Triassic cynodont preserving a natural endocast. *Journal of Vertebrate Plaeontology* **42**(3), e2174441.
https://doi.org/10.1080/02724634.2023.2174441
PUSCH, L.C., PONSTEIN, J., KAMMERER, C.F. & FRÖBISCH, J. 2020. Novel endocranial data on the early therocephalian *Lycosuchus vanderrieti* underpin high character variability in early theriodont evolution. *Frontiers in Ecology and Evolution* **7**, 464.
https://www.frontiersin.org/article/10.3389/fevo.2019.00464
RODRIGUES, P.G., RUF I. & SCHULTZ ,C.L. 2013. Digital reconstruction of the otic region and inner ear of the non-mammalian cynodont *Brasilitherium riograndensis* (Late Triassic, Brazil) and its relevance to the evolution of the mammalian ear. *Journal of Mammalian Evolution* **20**, 291–307.
DOI: 10.1007/s10914-012-9221-2
RODRIGUES, P.G., RUF, I. & SCHULTZ, C.L. 2014. Study of a digital cranial endocast of the nonmammaliaform cynodont *Brasilitherium riograndensis* (Later Triassic, Brazil) and its relevance to the evolution of the mammalian brain. *Paläontologische Zeitschrift* **88**, 329–352.
https://doi.org/10.1007/s12542-013-0200-6
ROMANO, M. & MANUCCI, F. 2019. Resizing *Lisowicia bojani*: volumetric body mass estimate and 3D reconstruction of the giant Late Triassic dicynodont. *Historical Biology* **33**, 474–479.
ROWE, T.B., MACRINI, T.E. & LUO, Z-X. 2011. Fossil evidence on origin of the mammalian brain. *Science* **332**, 955–957.
https://doi.org/10.1126/science.1203117
RUBEN, J. 1996. Evolution of endothermy in mammals, birds and their ancestors. **In**: Johnston, I.A. & Bennett, A.F. (eds), *Animals and Temperature: Phenotypic and Evolutionary Adaptation*, 347–376. Cambridge, Cambridge University Press.
RUBIDGE, B.S. 1995. Biostratigraphy of the Beaufort Group (Karoo Supergroup). *South African Committee for Stratigraphy Biostratigraphic Series* **1**, 1–46.
RUBEN, J.A., HILLENIUS, W.J., KEMP, T.S. & QUICK, D.E. 2012. The evolution of mammalian endothermy. **In**: Chinsamy-Turan, A. (ed.), *Forerunners of Mammals: Radiation, Histology, Biology*, 272–286. Bloomington, Indiana University Press.
SIDOR, C.A., KULIK, Z.T. & HUTTENLOCKER, A.K. 2022. A new bauriamorph therocephalian adds a novel component to the Lower Triassic tetrapod assemblage of the Fremouw Formation (Transantarctic Basin) of Antarctica. *Journal of Vertebrate Paleontology* **41**, e2081510.
SIGURDSEN, T. 2006. New features of the snout and orbit of a therocephalian therapsid from South Africa. *Acta Palaeontologica Polonica* **51**(1), 63–75.
http://app.pan.pl/acta51/app51-063.pdf
SIGURDSEN, T., HUTTENLOCKER, A.K., MODESTO, S.P., ROWE, T.B. & DAMIANI, R. 2012. Reassessment of the morphology and paleobiology of the therocephalian *Tetracynodon darti* (Therapsida), and the phylogenetic relationships of Baurioidea. *Journal of Vertebrate Paleontology* **32**, 1113–1134.
SMITH, R.M.H. & BOTHA-BRINK, J. 2014. Anatomy of a mass extinction: sedimentological and taphonomic evidence for drought-induced die-offs at the Permo-Triassic boundary in the main Karoo Basin, South Africa. *Palaeogeography, Palaeoclimatology, Palaeoecology* **15**, 99–118.
https://doi.org/10.1016/j.palaeo.2014.01.002
SMITH, R.M.H., RUBIDGE, B.S. & VAN DER WALT, M. 2012. Therapsid biodiversity patterns and paleoenvironments of the Karoo Basin, South Africa. **In**: Chinsamy-Turan, A. (ed.), *Forerunners of Mammals: Radiation, Histology, Biology*, 31–62. Bloomington, Indiana University Press.
VAN DEN HEEVER, J.A. 1994. The cranial anatomy of the early Therocephalia (Amniota: Therapsida). *Annals of the University of Stellenbosch* **1994**, 1–59.
VIGLIETTI, P.A., BENSON, R.B.J., SMITH, R.M.H., BOTHA, J., KAMMERER, C.F., SKOSAN, Z., BUTLER, E., CREAN, A., ELOFF, B., KAAL, S., MOHOI, J., MOLEHE, W., MTALANA, N., MTUNGATA, S., NTHERI, N., NTSALA, T., NYAPHULI, J., OCTOBER, P., SKINNER, G., STRONG, M., STUMMER, H., WOLVAARDT, F.P. & ANGIELCZYK, K.D. 2021. Evidence from South Africa for a protracted end-Permian extinction on land. *Proceedings of the National Academy of Sciences of the United States of America* **118**(17), e2017045118.
WATSON, D.M.S. 1931. On the skeleton of a bauriamorph reptile. *Proceedings of the Zoological Society of London* **1**, 1163–1205.